

IDENTIFICATION OF THE CALMODULIN BINDING DOMAIN OF CONNEXIN43*

^aYubin Zhou, ^aWei Yang, ^cMonica M. Lurtz, ^bYiming Ye, ^aYun Huang, ^aHsiau-Wei Lee,
^bYanyi Chen, ^cCharles F. Louis, and ^aJenny J. Yang

From the ^aDepartment of Chemistry, Georgia State University, Atlanta, GA 30303 USA; the ^bProteomics Laboratory, Biotechnology Core Facility Branch, Centers for Disease Control and Prevention, 1600 Clifton Rd. Mail Stop G-36, Atlanta, GA 30333; and the ^cDepartment of Cell Biology and Neuroscience, University of California, 900 University Avenue, Riverside, CA 92521, USA

Running Title: Interaction of Calmodulin with Connexin 43

Address corresponding to: Jenny J. Yang, Department of Chemistry, Georgia State University University Plaza, Atlanta, Georgia 30302 USA, Tel. 404-413-5520; Fax. 404-413-5551; Email: chejy@langate.gsu.edu

Calmodulin (CaM) has been implicated in mediating the Ca²⁺-dependent regulation of gap junctions. This report identifies a CaM-binding motif comprising residues 136-158 in the intracellular loop of Cx43. A 23-mer peptide encompassing this CaM-binding motif was shown to bind Ca²⁺-CaM with 1:1 stoichiometry by using various biophysical approaches, including surface plasmon resonance, circular dichroism, fluorescence spectroscopy and NMR. Far UV circular dichroism studies indicated that the Cx43-derived peptide increased its α -helical contents on CaM binding. Fluorescence and NMR studies revealed conformational changes of both the peptide and CaM following formation of the CaM:peptide complex. The apparent dissociation constant of the peptide binding to CaM in physiologic K⁺ is in the range of 0.7-1 μ M. On binding of the peptide to CaM, the apparent K_d of Ca²⁺ for CaM decreased from $2.9 \pm 0.1 \mu$ M to $1.6 \pm 0.1 \mu$ M, and the Hill Coefficient n_{Hill} increased from 2.1 ± 0.1 to 3.3 ± 0.5 . Transient expression in HeLa cells of two different mutant Cx43-EYFP constructs without the putative Cx43 CaM-binding site eliminated the Ca²⁺-dependent inhibition of Cx43 gap junction

permeability, confirming that residues 136-158 in the intracellular loop of Cx43 contains the CaM binding site that mediates the Ca²⁺-dependent regulation of Cx43 gap junctions. Our results provide the first direct evidence that CaM binds to a specific region of the ubiquitous gap junction protein Cx43 in a Ca²⁺-dependent manner, providing a molecular basis for the well characterized Ca²⁺-dependent inhibition of Cx43-containing gap junctions.

Gap junctions comprise the intercellular channels that mediate the cell-to-cell transfer of small molecules including metabolites, second messengers and ions in mammalian cells (1). Gap junctions are composed of two hemichannels (termed connexons) with each comprised of six connexin (Cx) subunits. The connexon from one cell joins in mirror symmetry with another connexon of the apposing cell. To date, at least 20 connexin genes have been identified in the human genome with connexin43 (Cx43) the most ubiquitous connexin (2).

Gap junctions have been shown to be regulated by intracellular Ca²⁺ concentration ([Ca²⁺]_i) (3) that Peracchia and others have shown to be likely mediated by CaM

interacting directly with the connexin proteins (4,5). We have shown previously that cell-to-cell communication in lens epithelial cell cultures is inhibited by elevated $[Ca^{2+}]_i$. Specifically, cell-to-cell transfer of the fluorescent dye AlexaFluor594 was half-maximally inhibited at ~ 300 nM $[Ca^{2+}]_i$ in lens cell cultures and this inhibition was prevented by preincubation of these cultures with CaM antagonists (6,7), consistent with earlier reports that elevated $[Ca^{2+}]_i$ increased internal electrical resistance in the lens that was prevented by preincubation with CaM antagonists (6). Indeed, this action of Ca^{2+} in lens cell cultures is due in part to the inhibition of Cx43, the major connexin in these cell cultures. It has demonstrated that Cx43-transfected HeLa cells exhibiting a similar Ca^{2+} -dependent inhibition appears to be CaM-mediated (8). The rapid onset of this Ca^{2+} -dependent inhibition of cell-to-cell communication (within seconds) suggests that this is mediated by a direct interaction of CaM with the connexin protein rather than being mediated via the action of a CaM-dependent protein kinase. Indeed, the Ca^{2+} -dependent binding of CaM to rat Cx32 (5), fish Cx35, mouse Cx36 (9) and Cx50 (10) have been reported. Two cytoplasmic CaM binding domains, with one site ($K_d = 27$ nM) in the N-terminus and the other site ($K_d = 1.2$ μ M) in the C-terminal region have been identified in Cx32 (5), whereas a single CaM binding site ($K_d: 11-72$ nM) was identified in the C-terminus of Cx35 and Cx36 (9).

Each Cx43 monomer consists of four highly-conserved transmembrane segments, a short N-terminal cytoplasmic region, one intracellular and two extracellular loops, as well as a C-terminal tail (Fig. 1A). Variability in sequence homology across different connexin types is greatest in the intracellular loop and C-terminus. Efforts to map the potential CaM binding sites in Cx43

have led to conflicting results. Torok *et al* reported the binding of the fluorescent CaM derivative (TA-CaM) to the N-terminal (aa 1-16) region of Cx43 with a dissociation constant of 1.2 μ M (5). However, Duffy *et al* were unable to detect any interaction of CaM with a peptide spanning the first 21 amino acids of the N-terminus (11). Both groups, nevertheless, failed to detect the binding of CaM to peptides derived from the C-terminal tail (aa 314-325; aa 336-350; aa 346-360) or the intracellular loop (aa 95-114; aa 123-136; aa 119-144). These results suggest that the interaction of CaM with Cx43 might occur via other regions of the intracellular loop. Interestingly, by using the CaM binding database server (12), we have predicted a potential CaM binding site with high predictive score in the second half of the intracellular loop of Cx43 (aa 136-158) that has not been tested before (Fig. 1). In the present study, we have applied a variety of biophysical approaches to examine the binding of CaM to this sequence. Our findings strongly suggest that Ca^{2+} effects the inhibition of Cx43 via a Ca^{2+} -dependent interaction between the CaM and residues 136-158 of this ubiquitous gap junction protein.

Experimental Procedures

Bioinformatic Analyses and Prediction of CaM-Binding Site in Connexins - The topology and orientation of transmembrane regions of rodent connexin 43 were predicted on the basis of the consensus results using four different programs including SOSUI (13), TMHMM (14), MEMSAT (15), and HMMTOP (16). The potential CaM binding sites were predicted using the CaM target database based on criteria that included the distribution of hydrophobic and basic residues, the propensity to form α -helix, and the hydrophobicity of the sequence, that are

common to more than 100 CaM target sequences (12).

Peptide Synthesis, Protein Expression and Purification - The peptide Cx43₁₃₆₋₁₅₈ (Ac-¹³⁶KYGIEEHGKVKMRGGLLRITYIIS¹⁵⁸-

NH₂) was synthesized by Sigma-Genosys (The Woodlands, Tx, USA) and purified by preparative reversed-phase HPLC with purity >95%. A randomized control peptide (Ac-LGGEYLVTMESKIHGKGRIGYR-NH₂) with the same composition of amino acids but arranged in a different order with no predicted CaM binding capacity (12) was similarly synthesized. Two other peptides with lower predictive scores, one in the N-terminal part of the intracellular loop region (Ac⁸⁶SVPTLLYLAHVYVMRKEEKLN¹⁰⁷-NH₂) and the other in the C terminus region (Ac²²⁴

NIIELFYVFFKGVKDRVKGRSDPY²⁴⁷-NH₂), were also synthesized. The molecular weight of the synthetic peptides were determined by matrix-assisted laser desorption/ionization time-of-flight mass spectrometry. To mimic the native protein environment and eliminate extra charges, the designed peptides were blocked at the N-termini with an acetyl group and at the C-termini with an amide group.

Recombinant rat CaM was expressed in *E. coli* strain BL21(DE3)pLysS transformed with the plasmid pET7-CaM that harbors the synthetic CaM gene (17). pET7-CaM transformed cells were grown in LB medium to obtain unlabeled CaM. ¹⁵N-labeled CaM was expressed in SV minimal medium using 0.5 g/L ¹⁵NH₄Cl (Cambridge Isotope Laboratories, MA, USA) as the sole nitrogen source. Bacterially-expressed CaM was purified by phenyl-Sepharose (Sigma-Aldrich, MO, USA) chromatography as previously described (18). The purity of CaM was examined by mass spectrometry or SDS-PAGE (supplemental Fig. 1). The concentration of CaM was determined by

UV spectroscopy using the ϵ_{276} of 3,030 M⁻¹ cm⁻¹ (19).

Dansyl CaM was prepared according to the method of Johnson *et al* (20) with slight modifications. Briefly, rat CaM was dansylated in the dark by mixing 1 ml protein (1 mM) with a 5-fold molar excess of dansyl chloride (dissolved in 1:1 acetone/ethanol) in 10 mM Mops, 100 mM KCl, 1 mM CaCl₂, pH 7.0 for 16 h at 4 °C. The reaction mixture was then extensively dialyzed against 10 mM Tris, 100 mM KCl at pH 7.4 to remove the residual free dansyl chloride. The modification of CaM by dansyl chloride was confirmed by ESI-MS with an increase in the molecular mass of +233. The bound dye concentration was determined by using the ϵ_{335} of 3980 M⁻¹ cm⁻¹ (20). An average of ~0.8 mol of the dansyl chromophore was incorporated per mol of CaM.

Plasmid construction and Transient Protein Expression - The wild type (wt) Connexin 43-EYFP construct (Cx43-EYFP) was a generous gift of Dr. Xiaohua Gong (UC Berkeley, CA). The mutant Cx43-EYFP constructs Cx43_{K146E, R148E}-EYFP double mutant, and Cx43_{M147Q, L151E, I156E}-EYFP triple mutant were synthesized by PCR mutational insertion using the following primers for Cx43_{K146E, R148E}-EYFP: forward GGC AAG GTG GAA ATG GAG GGC GG, reverse GTG CTC TTC AAT CCC GTA CTT G; and for Cx43_{M147Q, L151E, I156E}--EYFP: forward ACC TAC GAA ATC AGC ATC CTC TTC AAG, reverse TCT CAG TTC GCC GCC CCT CTG TTT CAC. Resultant constructs were verified by sequencing. Plasmid DNA was prepared for transfection by transformation into TOP10 competent cells (Invitrogen, Carlsbad, CA) and growing overnight on an LB agar supplemented with Kanamycin (0.1g/L), a single transformed colony was grown overnight in LB medium supplemented with Kanamycin (0.1g/L), and purified using the

Qiagen (Valencia, CA) Endo-Free Plasmid Maxi Kit per manufacturer's instructions. Plasmid concentrations were quantified using UV/Vis spectroscopy (260nm/280nm ratio, DU 640 Spectrophotometer, Beckman-Coulter, Fullerton, CA). Connexin-deficient HeLa cells were grown on glass coverslips in DMEM (with 44 mM NaHCO₃, pH 7.2) supplemented with 10%v/v FBS, 100 U/ml penicillin and 0.1 mg/ml streptomycin in a humidified 37°C incubator with 5% CO₂ to about 80% confluence. Transient transfection of HeLa cells was done using Lipofectamine 2000 in OptiMEM I reduced serum medium (Invitrogen, Carlsbad, CA) per manufacturer's instructions. 1 µg plasmid DNA was used per 35 mm culture dish, and 4 µl Lipofectamine 2000 per 1 µg DNA.

Surface Plasmon Resonance Measurements

- Real time binding assays were performed using surface plasmon resonance (SPR) at the Center for Disease Control and Prevention (Atlanta, GA, USA) on a Biacore 3000 system (Biacore AB, Uppsala, Sweden). CaM (500 nM in 10 mM sodium formate, pH 3.5) was directly immobilized onto the sensor chip CM5 using an amine coupling kit as described by the manufacturer. Varying concentrations of synthetic peptide were subsequently injected over the sensor surface at a flow rate of 50 µL/min in binding buffer (5 mM Ca, 100 mM KCl, 50 mM Tris-HCl, pH 7.4). Two minutes later, peptide-free binding buffer was injected to monitor the dissociation process. All measurements were carried out in parallel using two cells, one with immobilized CaM and the other as blank control with the carboxylated dextran matrix deactivated. The binding of peptide to CaM-immobilized flow cells was corrected accordingly from binding to control flow cells. The sensor chip was regenerated using 10 mM glycine, pH 2.2. The binding data

were analyzed using the BIAevaluation software with the 1:1 Langmuir fitting model.

Circular Dichroism Spectroscopy - Circular dichroism spectra were acquired in the far UV (190-260 nm) or near UV region (250-340 nm) on a Jasco-810 spectropolarimeter at room temperature using a 1 cm path length quartz cuvette. All spectra presented were averaged from 10-20 scans. The background signals from the corresponding buffers were subtracted from the sample signals. The far UV CD spectra of the peptide in different percentages of trifluoroethanol (TFE) were obtained using 10 µM of the peptide in 10 mM Tris-HCl, 10 or 100 mM KCl, pH 7.4. In the peptide titration of CaM experiment, 2-5 µL aliquots of the peptide stock solution (150 µM in 10 mM Tris-HCl, 10 or 100 mM KCl, pH 7.4) was gradually added into a 2-mL solution containing 1-2 µM CaM in the same buffer with 5 mM CaCl₂ or 5 mM EGTA. The signals from the peptide itself were subtracted. All the measurements were carried out in at least triplicates. The binding constants of the synthetic peptide to CaM were obtained with a 1:1 binding model by fitting the following equation (Eq. 1):

$$f = \frac{([CaM]_T + [P]_T + K_d) - \sqrt{([CaM]_T + [P]_T + K_d)^2 - 4[CaM]_T[P]_T}}{2[CaM]_T} \quad (1)$$

where f is the fractional change of CD signals at 222 nm, K_d is the dissociation constant for the peptide, and $[P]_T$ and $[CaM]_T$ are the total concentrations of the synthetic peptide and CaM, respectively. The secondary structure contents of the peptides or proteins were calculated with the online secondary structure prediction server DICHROWEB that integrates analysis algorithms such as SELCON, CONTINLL, CDSSTR and K2D (21). Near UV CD spectra were recorded with protein/peptide concentration of 80-100 µM in 10 mM Tris-

HCl, 100 mM KCl, pH 7.4 with 5 mM Ca²⁺ or 5 mM EGTA.

Steady-State Fluorescence Measurements - Steady-state fluorescence spectra were recorded using a QM1 fluorescence spectrophotometer (PTI) with a xenon short arc lamp at ambient temperature. Tyrosine fluorescence was monitored using excitation at 277 nm and emission at 307 nm with 2-4 nm bandpasses. The Ca²⁺ binding constants were determined by titrating the CaM (8 μM) or 1:1 CaM-peptide mixture (8 μM) in 1 mM EGTA, 100 mM KCl, 50 mM Tris-HCl, pH 7.4 with 1-5 μL aliquots of 10 mM Ca²⁺ stock solution in the same buffer containing the same concentrations of CaM and peptide. The pH change (0.03 to 0.04) was minimal during the titration process. To obtain accurate Ca²⁺ concentrations during the titration, the Ca²⁺ concentration at each point was determined with the Ca²⁺ dye Oregon Green 488 BAPTA-5N (0.2 μM; K_d = 20 μM; Invitrogen) with excitation at 492 nm and the emission at 520 nm. The ionized Ca²⁺ concentration was subsequently calculated according to the Equation 2:

$$[Ca^{2+}] = K_d \frac{F - F_{\min}}{F_{\max} - F} \quad (2)$$

where F is the fluorescence intensity of the dye at each titration point, F_{min} and F_{max} are the intensities of the Ca²⁺-free and the Ca²⁺-saturated dye, respectively. The Ca²⁺ titration of CaM data was fit to the nonlinear Hill equation (Eq. 3):

$$f = \frac{[M]^n}{K^n + [M]^n} \quad (3)$$

Where, f is the relative signal change observed during the experiment; [M] is the concentration of free Ca²⁺; K refers to dissociation constants of Ca²⁺; and n is the Hill coefficient.

For dansyl-CaM fluorescence measurement, 1 mL solution containing 1-2 μM dansyl-CaM in 10 mM Tris-HCl, 100 mM KCl, pH 7.4 with 5 mM Ca²⁺ or 5 mM

EGTA was titrated with 5-10 μL aliquots of the peptide stock solution (10 μM) in the same buffer. Fluorescence spectra was recorded using an excitation wavelength of 335 nm and collecting the fluorescence emission between 400 and 600 nm. Slit widths were set at 4-8 nm.

NMR Spectroscopy - All NMR experiments were performed using either Varian Inova 500 or 600 MHz spectrometers. NMR spectra were acquired with a spectral width of about 13 ppm in the ¹H dimension and 36 ppm in the ¹⁵N dimension at 35 °C. For the (¹H, ¹⁵N)-HSQC experiment, 0.5 mM ¹⁵N uniformly labeled CaM was titrated with 10-20 μL aliquots of the peptide stock solution (2.1 mM) in a buffer consisting of 10% D₂O, 100 mM KCl, 50 mM Tris-HCl with 10 mM EGTA or 10 mM Ca²⁺. The pH values of both sample solutions were carefully adjusted to 7.4 with trace amount of 2M KOH. NMR data were processed using the FELIX98 program (Accelrys).

Dye Transfer Assay – Confluent monolayers of HeLa cells grown on glass coverslips were loaded with the Ca²⁺ indicator Fura-2 AM (5 μM) in 2 ml HBSS⁺⁺ buffer (containing 1.8 mM Ca²⁺, with added 10 mM HEPES, 5 mM NaHCO₃, pH 7.2), then transferred to a microincubation chamber (model MSC-TD, Harvard Apparatus, Holliston, MA) as described previously (8). Imaging of intracellular Ca²⁺ was performed with a Nikon TE300 (Nikon Inc., Melville, NY) inverted microscope equipped with Nikon filter blocks for Fura-2 emission and AF594 optics (Chroma Technology Corp, Rockingham, VT), a Metaltek filter wheel (Metaltek Instruments, Raleigh, NC) housing excitation filters for Fura-2, a 75 watt xenon short arc lamp, a Hamamatsu CCD digital camera (Hamamatsu Corporation, Bridgewater, NJ), and supported on a vibration isolation table

(Technical Manufacturing, Peabody, MA). $[Ca^{2+}]_i$ was measured ratiometrically ($\lambda_{340}/\lambda_{380}$) with Fura-2 throughout each experiment in the injected cell and the cells adjacent to the injected cell, and Ca^{2+} concentrations determined as described previously (7). MetaFluor software (Universal Imaging Corp., Downingtown, PA) was used for data collection. Micropipettes (borosilicate glass capillaries: 1 mm O.D., 0.75 mm I.D, 100 μ m internal microfilament; Dagan Corporation, Minneapolis, MN) were pulled on a Flaming/Brown-type pipette puller (P-87; Sutter Instruments, Novato, CA). Micropipettes had tip diameters of <1 μ m and resistances of ~100-300 M Ω when filled with AlexaFluor 594 (1 mM) dissolved in deionized water. The micropipette was positioned with a low-drift hydraulic micromanipulator (MW-3; Narishige, Greenvale, NY), and AlexaFluor 594 was microinjected iontophoretically using a train of 5-ms current pulses applied every 100 ms for 60 s (3 s total injection time) at ambient temperature. If the micropipette became plugged, it was replaced with a new micropipette, and the data from such a partial injection were excluded from the analysis. Current was generated with a Duo 773 (World Precision Instruments, Sarasota, FL). Current duration, magnitude, and polarity were controlled with an A310 Accupulser pulse generator (World Precision Instruments, Sarasota, FL). Digitized images of AlexaFluor594 cell-to-cell transfer were recorded 2 min following the iontophoretic injection of fluorescent dye. A sustained elevation in $[Ca^{2+}]_i$ was effected by adding 1 μ M ionomycin to the medium, then 2 min later increasing the extracellular $[Ca^{2+}]$ from 1.8 mM to 21.8 mM.

Results

Identification of a CaM-Binding Region in the Intracellular Loop Sequence of the Gap Junction Protein Cx43 - Using a search program for CaM-binding sites (12), a putative CaM binding region with high predictive score was identified in the intracellular loop (¹³⁶KYGIEEHGKVKMRGGLLRTYIIS¹⁵⁸) of Cx43. In addition, two other stretches of sequences with lower predictive score, one at the N-terminal part of the intracellular loop and the other at the C-terminus, were detected (Fig. 1A). A common feature of the CaM binding regions is a number of hydrophobic residues interspersed with positively charged residues (≥ 3), typically forming a 1-5-10, 1-8-14 or 1-16 patterns of hydrophobic residues (12,22). These regions are normally comprised of 12-30 continuous amino acids with a strong propensity to form an amphipathic helical structure. The putative CaM binding region of Cx43, aa residues 136-158, exhibits a 1-5-10 hydrophobic residue motif (Fig. 1B lower) as reported in other well-characterized CaM targeting proteins such as CaM Kinase I (23), CaM Kinase II (24), MARCKS (25) and synapsin (26). Similar to previously reported CaM-binding sequences (12,22), an α -helical wheel representation of the predicted sequence in Cx43 shows that the positively charged residues segregate on one side of the wheel while the hydrophobic residues segregate on the other side when the sequence forms an α -helical structure (Fig. 1B). The randomized control peptide for residues 136-158 exhibited no CaM binding potential using the search program for CaM binding sites (data not shown).

The ability of peptide Cx43₁₃₆₋₁₅₈ corresponding to Cx43 residues 136-158 to form an α -helical structure (Fig 1B) was evaluated by monitoring its secondary structure using far UV CD in the presence of

varying concentrations of trifluoroethanol (TFE). In aqueous solution, the peptide Cx43₁₃₆₋₁₅₈ was largely unstructured with a negative maximum at 197 nm. However, when the TFE concentration was increased to 20 % it started to adopt an α -helical structure (12%), with two major troughs at 208 nm and 222 nm observed in the CD spectra. The helical content increased to 40% in 40% TFE and to 55% in 80% TFE (Fig. 2). TFE, with a dielectric constant one third that of water is capable of strengthening intramolecular hydrogen bonding (27), and is known to induce and stabilize the intrinsic secondary structures in peptides, possibly by mimicking the hydrophobic environment of these peptide regions in the intact protein (28-30). Several CaM-binding peptides have been reported to adopt similar α -helical structures in TFE solvent as occurs following formation of the CaM-peptide complex (31,32). These results support our prediction that this Cx43₁₃₆₋₁₅₈ peptide possesses a strong α -helical-forming propensity.

Secondary and Tertiary Structure Changes Induced by Peptide Binding - As described above, the binding of CaM to CaM-binding peptides typically induces the formation of α -helical structure in these peptides (33). As seen in Fig. 3A, the addition of a 1:1 molar equivalent of peptide to Ca²⁺-CaM results in an approximately 10% more negative signal in the spectrum. Since the α -helical content of CaM typically does not increase upon peptide binding (33), the observed net increase in the CD signal could be reasonably attributed to CaM-bound Cx43₁₃₆₋₁₅₈. The difference spectrum, obtained by subtracting the Ca²⁺-CaM spectrum from the Ca²⁺-CaM-peptide spectrum, showed two major troughs at 208 nm and 224 nm, which is strikingly different from the random coiled structure of the peptide alone (Fig. 3B). Deconvolution of

this difference spectra revealed that the CaM-bound Cx43₁₃₆₋₁₅₈ had ~35% helical structure, which is comparable to the helical content of this peptide in 40% TFE (Fig. 2). The Cx43₁₃₆₋₁₅₈ binding-induced CD signal change enabled us to measure the peptide binding affinity of CaM. As shown in the inset of Fig. 3B, the signal changes are maximal when the Cx43₁₃₆₋₁₅₈:CaM ratio was approximately 1:1 and the fitting curves provided an apparent K_d of 100 ± 20 nM ($n = 3$) in 10 mM KCl and 750 ± 120 nM ($n = 3$) in 100 mM KCl (Table 1) in the presence of 1 mM Ca²⁺. The decrease in K_d at higher salt concentration suggests that electrostatic interactions might play an important role in the interaction of Cx43₁₃₆₋₁₅₈ with CaM. In the presence of 1 mM EGTA, no significant difference in the far UV CD spectra was detected after the addition of a 1:1 molar equivalent of Cx43₁₃₆₋₁₅₈ to CaM (Fig. 3A) suggesting that the peptide is unable to interact with CaM or the binding is much weaker in the absence of Ca²⁺.

Near UV CD spectroscopy was conducted to examine the tertiary packing around aromatic residues of CaM, Cx43₁₃₆₋₁₅₈ and the CaM-Cx43₁₃₆₋₁₅₈ complex (Fig. 3). Cx43₁₃₆₋₁₅₈ exhibited negligible signal, but the addition of Cx43₁₃₆₋₁₅₈ to Ca²⁺-CaM resulted in the appearance of more negative ellipticity (Fig. 3C). Both CaM and the synthetic peptide do not contain any tryptophan but each contains two tyrosine residues. The prominent band above 275 nm is likely due to the tyrosine residues in the C-terminus region of CaM (Y99 and Y138), while the two peaks at 262 nm and 268 nm are likely due to the nine phenylalanine residues in CaM (34). The difference spectrum obtained by subtracting the Ca²⁺-CaM spectrum from that of Ca²⁺-CaM-Cx43₁₃₆₋₁₅₈ (Fig. 3D) showed a prominent band between 275 and 279 nm, which is most likely due to the immobilization of at least one of the two tyrosine residues in the

Cx43₁₃₆₋₁₅₈ peptide complex (which contains no tryptophan) following its binding to CaM. The contribution of signals from the CaM tyrosine residue is less likely to be dominant although both CaM and Cx43₁₃₆₋₁₅₈ contain two tyrosine residues making it difficult to unambiguously differentiate the contribution from each macromolecule in the spectra. The Y99 and Y138 in CaM are located in the C-terminus EF-loops where the local structures of the Ca²⁺-bound EF-loops have not been reported to be altered upon peptide binding in the currently known CaM-peptide complex despite the rearrangement of tertiary structures. Thus, the local environment of the CaM tyrosine is less likely to be significantly altered upon Cx43₁₃₆₋₁₅₈ peptide binding. No significant differences were observed between the spectra of apo-CaM and the 1:1 mixture of apo-CaM: Cx43₁₃₆₋₁₅₈ (Fig. 3C) further supporting the Ca²⁺-dependent binding of Cx43₁₃₆₋₁₅₈ to Ca²⁺-CaM and the resulting conformational changes in Cx43₁₃₆₋₁₅₈ revealed by the far UV CD studies.

Monitoring the CaM-Cx43₁₃₆₋₁₅₈ Interaction by Surface Plasmon Resonance Spectroscopy - The binding of Cx43₁₃₆₋₁₅₈ to CaM was further confirmed using surface plasmon resonance spectroscopy with CaM immobilized on the CM5 sensor chip. Fig. 4A shows the sensorgrams of successive peptide binding experiments. The peptide Cx43₁₃₆₋₁₅₈ rapidly associated with CaM in the presence of Ca²⁺. At the end of peptide injection, dissociation of the complex was observed during flushing of the chip with peptide-free running buffer. Analysis of the kinetic data inferred that the apparent K_d for the binding of Cx43₁₃₆₋₁₅₈ to CaM is approximately 1 μ M with a k_{off} rate of $5 \times 10^{-4} \text{ s}^{-1}$ in the presence of saturating amount of Ca²⁺ and 100 mM KCl. In contrast, no significant binding of Cx43₁₃₆₋₁₅₈ to CaM was detected in the presence of EGTA (Fig.

4A, dashed line). Furthermore, the control randomized Cx43₁₃₆₋₁₅₈ peptide that contained the same composition of amino acids as Cx43₁₃₆₋₁₅₈ did not exhibit specific binding in the presence of either Ca²⁺ or EGTA (Fig. 4B); the response units of these injections were not significantly higher than that of injection of the peptide through the underivatized CM5 chip surface. These results further confirm the Ca²⁺-dependent binding and specificity of Cx43₁₃₆₋₁₅₈ binding to CaM.

Peptide-Induced Conformational Changes Detected by Fluorescence Spectroscopy -

The tyrosine fluorescence intensity of Cx43₁₃₆₋₁₅₈ remained almost unchanged upon the addition of Ca²⁺. In contrast, the addition of Ca²⁺ enhanced the fluorescence intensity of both CaM and a 1:1 CaM-Cx43₁₃₆₋₁₅₈ mixture (2.3 and 1.7 fold respectively). The sum of the fluorescence intensities of Ca²⁺-CaM and Cx43₁₃₆₋₁₅₈ nearly equaled that of the Ca²⁺-CaM-Cx43₁₃₆₋₁₅₈ complex, suggesting that the fluorescence enhancement resulted primarily from the conformational change of the CaM upon Ca²⁺ binding. However, the blue shift of the maximal emission peak from 307 nm to 304 nm was observed when Cx43₁₃₆₋₁₅₈ bound to Ca²⁺-CaM (Fig. 5A), suggesting that the tyrosine environment (likely of those residues in the peptide as discussed above) became more hydrophobic after the formation of the CaM:Cx43₁₃₆₋₁₅₈ complex.

The dansyl fluorescence emission maxima, at \sim 510 nm, is well-separated from any intrinsic fluorescence arising from aromatic amino acid residues. Because of this, as well as fluorescent dye's great sensitivity to changing environment, fluorescent dye-labeled proteins including dansylated CaM have been widely used in studying the effect of protein-target interaction of ions, peptides, or drugs (20,35). As shown in Fig. 5B, Ca²⁺ binding

to dansyl-CaM resulted in an increase of the fluorescence intensity and an emission blue-shift from 510 to 497 nm indicating that the dansyl group moved to a more hydrophobic environment. The addition of Cx43₁₃₆₋₁₅₈ to Ca²⁺-dansyl-CaM resulted in a further 80% increase in dansyl fluorescence intensity and a further emission blue-shift to 477 nm, suggesting that the dansyl groups are located in an even more hydrophobic environment in the complex. In the absence of Ca²⁺, the dansyl fluorescence remained nearly unaltered when Cx43₁₃₆₋₁₅₈ was added to dansyl-CaM, indicating a Ca²⁺-dependent interaction of Cx43₁₃₆₋₁₅₈ with dansyl-CaM, thus supporting a model in which the interaction of Cx43₁₃₆₋₁₅₈ with CaM is Ca²⁺-dependent. In addition, the titration of dansyl-CaM with two other Cx43 peptides (Cx43₈₆₋₁₀₇ corresponding to residues 86-107 in Cx43 in the N-terminal region of the intracellular loop, and Cx43₂₂₄₋₂₄₇ corresponding to residues 224-247 in Cx43 in the C-terminus region) that have significantly lower predictive scores for CaM binding (Fig 1A) resulted in no significant fluorescence signal changes (Figs. 5C and 5D) indicating these peptides did not bind CaM. Titration data of CaM with Cx43₁₃₆₋₁₅₈ in 1 mM CaCl₂ resulted in apparent dissociation constants of 240 ± 10 nM in 10 mM KCl and 860 ± 20 nM in 100 mM KCl (Table 1) assuming a 1:1 CaM:Cx43₁₃₆₋₁₅₈ binding mode (Fig. 5B inset). These binding affinities are comparable to those obtained with far UV CD spectroscopy (Fig. 3); the differences in these values are likely attributable to the dansyl modification of CaM and/or the different methodologies used.

NMR Studies on the CaM-Peptide Interaction - It was important to demonstrate that there is in fact a direct interaction between the Cx43₁₃₆₋₁₅₈ and CaM. This was confirmed using NMR. As shown in Fig. 6A,

in the presence of Ca²⁺, a number of dispersed peaks of CaM underwent chemical shifts of greater than 0.05 ppm following the addition of Cx43₁₃₆₋₁₅₈. In contrast, only insignificant changes in several residues were observed upon the addition of Cx43₁₃₆₋₁₅₈ to CaM in the presence of 10 mM EGTA (Fig. 6B), again supporting the absence of any of interaction at physiological concentrations of K⁺ in the absence of Ca²⁺. In addition, the addition of the control randomized Cx43₁₃₆₋₁₅₈ peptide (see Experimental Procedure) resulted in only very minor changes in the CaM ¹⁵N-¹H HSQC spectra in the presence of either Ca²⁺ or EGTA (Fig. 6A). This latter result would appear to exclude the possibility of non-specific binding between the randomized peptide and CaM arising from the charge or hydrophobic interactions of certain residues, indicating the necessity of the specific arrangement of the Cx43₁₃₆₋₁₅₈ peptide sequence.

The NMR chemical shift resonances of Ca²⁺-CaM have been assigned by several groups (33,36,37). By following their movements during titration of CaM with Cx43₁₃₆₋₁₅₈ peptide, the dispersed peaks of the peptide-CaM complex have been unambiguously assigned. CaM has been known to activate downstream proteins by displacing autoinhibitory domains, remodeling the active sites, or inducing oligomerization in these proteins (38). The binding of CaM to target proteins and peptides has been reported to involve the N- and/or C-terminal domains of CaM (33,38-40). Analysis of the effects of peptide binding on the backbone amide chemical shifts of CaM could shed light on the underlying mode of interaction of the Cx43₁₃₆₋₁₅₈ peptide with CaM. The resonances that underwent chemical shifts of greater than 0.05 ppm in the peptide titration were present in both the N- to C-termini of CaM, including residues G25, T29, G33,

G40, A57, G61, D64, K77, K94, G98, G113, T117, G134, N137, A147 and K148 and possibly others since the assignment of the overlapped regions is still in progress (Fig. 6A and 6D). The movements of the residues that we were able to assign during the titration followed a similar chemical shift trend (Fig. 6C), suggesting a single binding process. Furthermore, the chemical shifts saturated when the Cx43₁₃₆₋₁₅₈ to CaM ratio exceeded 1.0 (Fig. 6C). These results demonstrated that the 1:1 Ca²⁺-dependent binding of Cx43₁₃₆₋₁₅₈ to CaM induces conformational changes in both the N- and C-terminal domains of CaM.

Effect of Cx43₁₃₆₋₁₅₈ on the Ca²⁺ Binding of CaM - To examine the effect of Cx43₁₃₆₋₁₅₈ on the Ca²⁺ binding properties of CaM, Ca²⁺ titrations were performed in the presence of the Ca²⁺ indicator Oregon Green 488 BAPTA-5N. The Ca²⁺-dependent change in the intrinsic tyrosine fluorescence of CaM in the presence of Cx43₁₃₆₋₁₅₈ was slightly left-shifted when compared to CaM alone (pCa₅₀ 5.8 ± 0.1 for the mixture *versus* 5.6 ± 0.1 for CaM; Fig. 7). Furthermore, the Ca²⁺-dependent change in the tyrosine fluorescence of the CaM:Cx43₁₃₆₋₁₅₈ mixture exhibited stronger positive cooperativity than that of CaM alone (Hill coefficients: 3.3 *versus* 2.1) for Ca²⁺ binding. It is well recognized that the Ca²⁺ affinity of CaM is significantly enhanced on binding to its receptor protein as a result of a slower dissociation rate of Ca²⁺ from CaM-receptor complex than from CaM alone (41-44). The dissociation of Ca²⁺ from CaM typically leads to the inactivation or inhibition of its bound protein (40) so slowing this dissociation would ensure that the CaM:Cx43 complex remains associated even during periods of frequent oscillation of [Ca²⁺]_i. Furthermore, a greater positive cooperativity for Ca²⁺ binding enables the

complex to respond to a narrower window of [Ca²⁺]_i with higher sensitivity.

Physiological effects of knocking out the putative CaM-binding site in Cx43. - Physiological experiments were conducted to confirm the results obtained using various biophysical approaches. Cell-to-cell dye transfer under resting and elevated intracellular Ca²⁺ concentration ([Ca²⁺]_i) in communication-deficient HeLa cells transiently transfected individually with either wtCx43-EYFP or one of two Cx43-EYFP intracellular loop mutants (CaM binding site knockouts) was used to demonstrate that CaM mediates the Ca²⁺-dependent inhibition of Cx43 by directly associating with the aa 136-158 region in Cx43.

HeLa cells transiently transfected with wtCx43-EYFP expressed large gap junction plaques at the cell-cell interface (Fig. 8A & D, left panels) as has been previously described (45); there was no significant intracellular expression of wtCx43-EYFP making it relatively straight forward to identify cells making gap junctions with adjacent cells (Fig 8A). In contrast both the Cx43_{K146E, R148E}-EYFP and Cx43_{M147Q, L151E, I156E}-EYFP CaM binding-deficient mutants expressed an abundance of protein when transfected in HeLa cells, most of which was in non-plasma membrane locations (Fig 8 B&F, C&G left panels, respectively) making it harder to identify cells making gap junctions with adjacent HeLa cells. Under resting [Ca²⁺]_i conditions (1.8 mM extracellular Ca²⁺ concentration and no ionomycin), cell-to-cell communication (i.e., AlexaFluor 594 cell-to-cell dye transfer) was measured between each pair of cells expressing the wtCx43-EYFP; every cell that contained EYFP fluorescence exhibited cell-to-cell transfer of injected dye indicating that Cx43-EYFP formed functional gap junctions (Fig 8I). In

contrast, only 31% of the double mutant Cx43_{K146E, R148E}-EYFP transfected HeLa cells and 32% of the triple mutant Cx43_{M147Q, L151E, I156E}-EYFP transfected HeLa cells exhibited cell-to-cell dye transfer (Fig 8I). These results indicated that a significant fraction of the mutant Cx43-EYFP transfected cells that exhibited EYFP fluorescence did not express functional gap junctions. This fits with the EYFP fluorescence data (Figs 8B & 8C) suggesting a significant fraction of the mutant Cx43-EYFP protein accumulates in non-plasma membrane locations in the transfected HeLa cells. Furthermore, mock-transfected HeLa cells did not exhibit cell-to-cell transfer of injected AlexaFluor 594 dye confirming that the cell-to-cell transfer exhibited by the wt Cx43-EYFP and mutant Cx43-EYFP transfected HeLa cells is gap junction mediated (Fig. 8D).

Addition of the membrane permeant polyether antibiotic ionomycin (1 μ M) and subsequent elevation of extracellular Ca^{2+} from 1.8 mM to 21.8 mM resulted in a significant ($p < 0.001$) increase of the $[\text{Ca}^{2+}]_i$ to concentrations known to inhibit Cx43-mediated cell-to-cell dye transfer in a CaM-dependent manner (7, 8). As shown in Fig. 8I, elevation of $[\text{Ca}^{2+}]_i$ in wtCx43-EYFP transiently transfected HeLa cells results in the inhibition of cell-to-cell dye transfer in all cells tested indicating that the addition of EYFP on the C-terminus of Cx43 did not affect the ability of elevated $[\text{Ca}^{2+}]_i$ to inhibit Cx43 gap junctions. In contrast, elevation of $[\text{Ca}^{2+}]_i$ in HeLa cells expressing the Cx43_{K146E, R148E}-EYFP double mutant or the Cx43_{M147Q, L151E, I156E}-EYFP triple mutant did not result in the inhibition cell-to-cell dye transfer (57% and 67% [respectively] of attempts resulted in dye transfer). The apparent increase in the percentage of injected cells inhibiting cell-to-cell dye transfer in elevated $[\text{Ca}^{2+}]_i$ versus resting $[\text{Ca}^{2+}]_i$ was not statistically significant

($p > 0.1$). There was no cell-to-cell transfer of dye when AlexaFluor 594 dye was injected into mock HeLa transfected cells under either resting or elevated $[\text{Ca}^{2+}]_i$ conditions (Fig. 8H).

Discussion

Indication of in vivo Interaction - In this report we provide evidence that a 23-mer peptide derived from the intracellular loop region residues 136-158 of the major gap junction protein Cx43, which has the highest predictive score of any region of Cx43 for binding to CaM (Fig. 1), binds CaM with high affinity in a Ca^{2+} -dependent manner. That intracellular CaM concentration is approximately 9 μ M (46), indicates that such an affinity would imply that this CaM-binding region of Cx43 would likely be at least half saturated with CaM when intracellular Ca^{2+} concentration is elevated to $\sim 1 \mu\text{M}$ and that this Ca^{2+} -dependent association accounts for the well described ability of Ca^{2+} to inhibit gap junctions (7). As indicated by our circular dichroism, fluorescence and NMR data (Figs. 4-6), the stoichiometry of Cx43₁₃₆₋₁₅₈ peptide:CaM binding is close to 1:1. To our knowledge, this report presents the first demonstration of a direct CaM-Cx43 interaction *in vitro*, which would explain our previous *in vivo* observation that preincubation of lens cell cultures or Cx43-transfected HeLa cells with CaM antagonists counteracts the intracellular Ca^{2+} -dependent inhibition of Cx43-containing gap junctions (6,7). These results clearly demonstrate that the Ca^{2+} -dependent inhibition of Cx43 gap junctions is mediated via the association of Ca^{2+} -CaM with the intracellular loop region of Cx43. In addition, our results support a mechanism of Cx43 regulation by CaM in which CaM first binds to Ca^{2+} , and then the Ca^{2+} -CaM complex associates with Cx43 to inhibit Cx43 gap junctions, rather than a stable

CaM-Cx43 complex in which Ca^{2+} binds to the complex which then effects the inhibition of Cx43 gap junctions.

A different model for the gating of Cx43 has been proposed by Delmar's laboratory (11) in which an intracellular gating element within the C-terminal domain of Cx43 interacts with a region of the Cx43 cytoplasmic loop in a pH-dependent manner. In that report Duffy *et al* used surface plasmon resonance, ELISA and NMR approaches to demonstrate that a portion of the C-terminal of Cx43 comprising amino acids 255-382 associated with a peptide corresponding to the second half of the Cx43 intracellular loop comprising amino acids 119-144 which was significantly enhanced by low pH. The results reported here for the inhibition of Cx43 by Ca^{2+} -CaM has an interesting corollary to this pH-dependent inhibition described by Duffy *et al* (11) in that binding of a portion of Cx43 C-terminus region or CaM to the cytoplasmic region of Cx43 inhibits this gap junction protein. However, while Sorgen *et al* (47) reported that dimerization of the Cx43 C-terminal region may be one of the structural changes involved in the pH regulation of Cx43, our data reported here indicate that Ca^{2+} -CaM and the intracellular loop peptide associate as a 1:1 complex; i.e. that a single Ca^{2+} -CaM binds to Cx43 (i.e. 6 Ca^{2+} -CaM per connexon hemichannel) to effect gap junction closure. Indeed while there is partial overlap of the C-terminal binding domain on the intracellular loop reported by Duffy *et al* (11) (residues 119-144) and the CaM binding domain (residues 136-158) reported here, it is clear that CaM will associate with a portion of Cx43 that is very close to the third transmembrane region of this connexins so it is well positioned to physically obstruct the gap junction pore.

As in any molecular study conducted *in vitro*, direct extrapolation between the data presented in this report using a peptide, and

the mechanisms of Ca^{2+} -CaM gating of Cx43 in intact cells needs to be made with caution. However, it is worth noting that there are several examples in the literature demonstrating that two molecular domains that associate in living cells also associate as separate domains *in vitro* (48,49). In the studies of CaM-target interaction, synthetic peptides have been widely used due to their excellent ability to mimic specific domains of native proteins (33,50-54). Indeed Peracchia *et al* (4,55) have shown that calmodulin is associated with gap junctions and plays a direct role in the chemical gating of Cx32-containing gap junctions. This was supported by data for CaM binding to Cx32 in which Török *et al* (5) identified two distinct CaM binding amino acid sequences. The sequence of one of these sites in the N-terminal domain of Cx32 contains a CaM binding motif common to a large class of CaM-dependent proteins (22); notably this N-terminal CaM binding sequence is absent in Cx43 (Fig. 1).

Indication of the Potential CaM-Cx43₁₃₆₋₁₅₈ Binding Mode - Through its reversible binding of Ca^{2+} and the resultant conformational changes, CaM is capable of interacting with over 300 target proteins to regulate a range of cellular events (56). Although the sequence identity among the CaM targeted sequences is low, all the consensus peptides for such sequences (18 to 26-mer peptides) possess common features including their ability to form amphipathic α -helices, containing 2-6 positively charged residues, and their pattern of bulky hydrophobic residues that anchor the peptides to the hydrophobic cleft of CaM. Our results demonstrate that the Cx43₁₃₆₋₁₅₈ sequence forms an α -helical structure in TFE as well as in the CaM-peptide complex, similar to other CaM-bound peptides (25,30,32,57,58). Two lysine and two arginine residues are contained in the

Cx43₁₃₆₋₁₄₈ sequence which has a high predictive score for CaM binding. The basic residues in the N-terminus of CaM-binding sequences have been proposed to ensure an antiparallel orientation of the peptide with respect to CaM (59), which is believed to optimize the electrostatic attraction between the basic residues of the peptide with negatively charged residues in CaM. In addition, the hydrophobic residues M₁₄₇-L₁₅₁-I₁₅₆ of the Cx43 peptide reflect the 1-5-10 type of CaM-binding pattern (Fig. 1), which is similar to the CaM-binding regions of CaMKI and CaMKII (12,22,57).

In addition to the formation of α -helical structure by the Cx43₁₃₆₋₁₅₈ peptide, the hydrophobicity of the peptide environment as well as the tertiary arrangement of the CaM are also changed following the formation of the CaM:Cx43₁₃₆₋₁₅₈ complex. As indicated by the near UV CD and tyrosine fluorescence studies, the chemical environment around the tyrosine residues is significantly perturbed following the binding of Cx43₁₃₆₋₁₅₈ to CaM. Furthermore, the significant blue shift and concomitant enhancement of fluorescence intensity induced by Cx43₁₃₆₋₁₅₈ binding to dansyl-CaM (Fig. 5B) suggests that the dansyl group in dansyl-CaM is shielded from the solvent and moves into a highly hydrophobic environment on binding to Cx43₁₃₆₋₁₅₈; similar changes have been observed for the binding of dansyl-CaM to other receptors (60-62). A number of the currently-assigned CaM resonances in the NMR ¹H-¹⁵N HSQC spectra exhibited chemical shifts movements ≥ 0.05 ppm. These residues were spread in both the N- and C-terminal domains of CaM as well as in the linker region, indicating a global conformational change occurred upon binding of the Cx43₁₃₆₋₁₅₈ peptide to CaM (Fig. 6D). Such a global changes of amide chemical shifts have also been reported in other CaM complexes such as Ca²⁺-CaM-

skeletal muscle myosin light chain kinase and Ca²⁺-CaM-CaMKI (33,63). Together these observations suggest that the Ca²⁺-CaM-Cx43₁₃₆₋₁₅₈ interaction might adopt the commonly seen wrapping-around mode of action (64).

In vivo functional analysis of the putative Cx43 CaM-binding site – Transient expression of a Cx43-EYFP construct without and with mutations in communication-deficient HeLa cells provided a system by which to test our biophysical data in a physiologic manner. Because CaM interaction with a protein requires both an electrostatic interaction and a hydrophobic interaction, we generated two Cx43 mutants - Cx43_{K146E, R148E}-EYFP that knocks out the Cx43 electrostatic interaction with CaM, and Cx43_{M147Q, L151E, I156E}-EYFP that knocks out the hydrophobic interaction of Cx43 with CaM. Transient expression of these EYFP-tagged Cx43 constructs was consistent with the anticipated results. The wtCx43-EYFP formed very large gap junction plaques and dye transfer was restricted to those cells expressing EYFP fluorescence (see Fig. 8A&E). With elevated [Ca²⁺]_i, these junctions were no longer dye coupled as reported by us previously with wt Cx43 that lacked the EYFP label.

As CaM has been implicated in Cx32 assembly at two stages of oligomerization (65), it was anticipated that the Cx43_{K146E, R148E}-EYFP and Cx43_{M147Q, L151E, I156E}-EYFP mutants would probably encounter problems reaching the plasma membrane, and perhaps even not form functional gap junctions. Indeed, although both of the mutant Cx43 proteins did express, the majority of the expressed protein was trapped inside the cell, very little of this protein appeared to reside in the plasma membrane, and no obvious gap junction plaques were observed (Figs. 8B & 8C).

Thus it was not anticipated that either of the mutants would exhibit cell-to-cell transfer of injected dye as reproducibly as we observed with the Cx43-EYFP. This proved to be the case because while in low ($\sim 1 \mu\text{M}$) $[\text{Ca}^{2+}]_i$, 100% of the wt Cx43-EYFP transfected HeLa cells exhibited cell-to-cell transfer of injected dye, only approximately 30% of each of the mutant-transfected HeLa cells appeared to be functional and exhibited cell-to-cell transfer of injected dye (Fig. 8I). However, while elevated $[\text{Ca}^{2+}]_i$ completely prevented cell-to-cell dye transfer between wt Cx43-EYFP transfected HeLa cells, elevated $[\text{Ca}^{2+}]_i$ was now unable to inhibit cell-to-cell dye transfer between HeLa cells transfected with these Cx43 mutants. Thus, knocking out the CaM binding capability of the residue 136-158 region of Cx43 abolished the Ca^{2+} -dependent inhibition of Cx43 gap junctions supporting our biophysical data that demonstrates that CaM mediates the Ca^{2+} -dependent inhibition of Cx43 via its interaction with residues 136-158 in this connexin.

In summary, we have identified a CaM binding sequence in the ubiquitous gap junction protein Cx43. This sequence resides

in a juxtamembrane region of the only intracellular loop of Cx43. Our results demonstrate a 1:1 Ca^{2+} -dependent CaM-Cx43 peptide interaction with an affinity in the submicromolar range. The binding of this peptide to CaM enhances the Ca^{2+} affinity of CaM approximately 2-fold. This biophysical result was confirmed in physiologic experiments with site directed mutations in the predicted CaM binding region of this connexin. These results explain the molecular basis of our previously reported Ca^{2+} -CaM-dependent regulation of both lens and Cx43-containing gap junctions via a direct interaction of CaM with this connexin protein (6,7). The data reported here confirms that this regulation is effected via the Ca^{2+} -dependent association of CaM with residues 136-158 of Cx43 that in turn effects a change in the structural organization of Cx43 such that gap junction permeability is significantly inhibited. Further elucidation of the structural changes within both CaM and Cx43, as well as the molecular basis of the Ca^{2+} -dependent regulation of the other lens connexins is the subject of ongoing investigations in this laboratory.

FOOTNOTES

* This research was supported by NIH grant EY-05684 to CFL and JY and GM62999 to JY. YZ is a fellow of the Molecular Basis of Disease Area of Focus at Georgia State University.

REFERENCES

1. Mathias, R. T., Rae, J. L., and Baldo, G. J. (1997) *Physiological reviews* 77(1), 21-50
2. Musil, L. S., Beyer, E. C., and Goodenough, D. A. (1990) *J Membr Biol* 116(2), 163-175
3. Noma, A., and Tsuboi, N. (1987) *J Physiol* 382, 193-211
4. Peracchia, C., Sotkis, A., Wang, X. G., Peracchia, L. L., and Persechini, A. (2000) *J Biol Chem* 275(34), 26220-26224
5. Torok, K., Stauffer, K., and Evans, W. H. (1997) *Biochem J* 326 (Pt 2), 479-483
6. Gandolfi, S. A., Duncan, G., Tomlinson, J., and Maraini, G. (1990) *Curr Eye Res* 9(6), 533-541

7. Churchill, G. C., Lurtz, M. M., and Louis, C. F. (2001) *Am J Physiol Cell Physiol* 281(3), C972-981
8. Lurtz, M. M., and Louis, C. F. (2003) *Am J Physiol Cell Physiol* 285(6), C1475-1482
9. Burr, G. S., Mitchell, C. K., Keflemariam, Y. J., Heidelberger, R., and O'Brien, J. (2005) *Biochem Biophys Res Commun* 335(4), 1191-1198
10. Zhang, X., and Qi, Y. (2005) *Arch Biochem Biophys* 440(2), 111-117
11. Duffy, H. S., Sorgen, P. L., Girvin, M. E., O'Donnell, P., Coombs, W., Taffet, S. M., Delmar, M., and Spray, D. C. (2002) *J Biol Chem* 277(39), 36706-36714
12. Yap, K. L., Kim, J., Truong, K., Sherman, M., Yuan, T., and Ikura, M. (2000) *J Struct Funct Genomics* 1(1), 8-14
13. Mitaku, S., Hirokawa, T., and Tsuji, T. (2002) *Bioinformatics* 18(4), 608-616
14. Krogh, A., Larsson, B., von Heijne, G., and Sonnhammer, E. L. (2001) *J Mol Biol* 305(3), 567-580
15. Jones, D. T. (1998) *FEBS Lett* 423(3), 281-285
16. Tusnady, G. E., and Simon, I. (2001) *Bioinformatics* 17(9), 849-850
17. Fruen, B. R., Black, D. J., Bloomquist, R. A., Bardy, J. M., Johnson, J. D., Louis, C. F., and Balog, E. M. (2003) *Biochemistry* 42(9), 2740-2747
18. Balog, E. M., Norton, L. E., Bloomquist, R. A., Cornea, R. L., Black, D. J., Louis, C. F., Thomas, D. D., and Fruen, B. R. (2003) *J Biol Chem* 278(18), 15615-15621
19. Wallace, R. W., Tallant, E. A., and Cheung, W. Y. (1983) *Methods Enzymol* 102, 39-47
20. Johnson, J. D., and Wittenauer, L. A. (1983) *Biochem J* 211(2), 473-479
21. Whitmore, L., and Wallace, B. A. (2004) *Nucleic Acids Res* 32(Web Server issue), W668-673
22. Rhoads, A. R., and Friedberg, F. (1997) *Faseb J* 11(5), 331-340
23. Clapperton, J. A., Martin, S. R., Smerdon, S. J., Gamblin, S. J., and Bayley, P. M. (2002) *Biochemistry* 41(50), 14669-14679
24. Rosenberg, O. S., Deindl, S., Sung, R. J., Nairn, A. C., and Kuriyan, J. (2005) *Cell* 123(5), 849-860
25. Yamauchi, E., Nakatsu, T., Matsubara, M., Kato, H., and Taniguchi, H. (2003) *Nature structural biology* 10(3), 226-231
26. Nicol, S., Rahman, D., and Baines, A. J. (1997) *Biochemistry* 36(38), 11487-11495
27. Yang, J. J., Buck, M., Pitkeathly, M., Kotik, M., Haynie, D. T., Dobson, C. M., and Radford, S. E. (1995) *J Mol Biol* 252(4), 483-491
28. Lehrman, S. R., Tuls, J. L., and Lund, M. (1990) *Biochemistry* 29(23), 5590-5596
29. Brokx, R. D., Scheek, R. M., Weljie, A. M., and Vogel, H. J. (2004) *J Struct Biol* 146(3), 272-280
30. Zhang, M., Yuan, T., and Vogel, H. J. (1993) *Protein Sci* 2(11), 1931-1937
31. Zhang, M., and Vogel, H. J. (1994) *Biochemistry* 33(5), 1163-1171
32. Zhan, Q. Q., Wong, S. S., and Wang, C. L. (1991) *J Biol Chem* 266(32), 21810-21814
33. Ikura, M., Clore, G. M., Gronenborn, A. M., Zhu, G., Klee, C. B., and Bax, A. (1992) *Science* 256(5057), 632-638
34. Martin, S. R., and Bayley, P. M. (1986) *Biochem J* 238(2), 485-490
35. LaPorte, D. C., Keller, C. H., Olwin, B. B., and Storm, D. R. (1981) *Biochemistry* 20(14), 3965-3972
36. Ikura, M., Spera, S., Barbato, G., Kay, L. E., Krinks, M., and Bax, A. (1991) *Biochemistry* 30(38), 9216-9228

37. Chou, J. J., Li, S., Klee, C. B., and Bax, A. (2001) *Nature structural biology* 8(11), 990-997
38. Hoefflich, K. P., and Ikura, M. (2002) *Cell* 108(6), 739-742
39. Elshorst, B., Hennig, M., Forsterling, H., Diener, A., Maurer, M., Schulte, P., Schwalbe, H., Griesinger, C., Krebs, J., Schmid, H., Vorherr, T., and Carafoli, E. (1999) *Biochemistry* 38(38), 12320-12332
40. Ikura, M., and Ames, J. B. (2006) *Proc Natl Acad Sci U S A* 103(5), 1159-1164
41. Johnson, J. D., Snyder, C., Walsh, M., and Flynn, M. (1996) *J Biol Chem* 271(2), 761-767
42. Kasturi, R., Vasulka, C., and Johnson, J. D. (1993) *J Biol Chem* 268(11), 7958-7964
43. Brown, S. E., Martin, S. R., and Bayley, P. M. (1997) *J Biol Chem* 272(6), 3389-3397
44. Olwin, B. B., Edelman, A. M., Krebs, E. G., and Storm, D. R. (1984) *J Biol Chem* 259(17), 10949-10955
45. Lai, A., Le, D. N., Paznekas, W. A., Gifford, W. D., Jabs, E. W., and Charles, A. C. (2006) *J Cell Sci* 119(Pt 3), 532-541
46. Black, D. J., Tran, Q. K., and Persechini, A. (2004) *Cell calcium* 35(5), 415-425
47. Sorgen, P. L., Duffy, H. S., Spray, D. C., and Delmar, M. (2004) *Biophys J* 87(1), 574-581
48. Sheng, M., and Sala, C. (2001) *Annu Rev Neurosci* 24, 1-29
49. Mayer, B. J. (2001) *J Cell Sci* 114(Pt 7), 1253-1263
50. Urbauer, J. L., Short, J. H., Dow, L. K., and Wand, A. J. (1995) *Biochemistry* 34(25), 8099-8109
51. Martin, S. R., Bayley, P. M., Brown, S. E., Porumb, T., Zhang, M., and Ikura, M. (1996) *Biochemistry* 35(11), 3508-3517
52. Xiong, L. W., Newman, R. A., Rodney, G. G., Thomas, O., Zhang, J. Z., Persechini, A., Shea, M. A., and Hamilton, S. L. (2002) *J Biol Chem* 277(43), 40862-40870
53. Kranz, J. K., Lee, E. K., Nairn, A. C., and Wand, A. J. (2002) *J Biol Chem* 277(19), 16351-16354
54. Ishida, H., and Vogel, H. J. (2006) *Protein Pept Lett* 13(5), 455-465
55. Peracchia, C. (2004) *Biochim Biophys Acta* 1662(1-2), 61-80
56. Berridge, M. J., Bootman, M. D., and Lipp, P. (1998) *Nature* 395(6703), 645-648
57. Meador, W. E., Means, A. R., and Quioco, F. A. (1993) *Science* 262(5140), 1718-1721
58. Yamniuk, A. P., and Vogel, H. J. (2004) *J Biol Chem* 279(9), 7698-7707
59. Osawa, M., Tokumitsu, H., Swindells, M. B., Kurihara, H., Orita, M., Shibamura, T., Furuya, T., and Ikura, M. (1999) *Nature structural biology* 6(9), 819-824
60. Gomes, A. V., Barnes, J. A., and Vogel, H. J. (2000) *Arch Biochem Biophys* 379(1), 28-36
61. Trost, C., Bergs, C., Himmerkus, N., and Flockerzi, V. (2001) *Biochem J* 355(Pt 3), 663-670
62. Turner, J. H., Gelasco, A. K., and Raymond, J. R. (2004) *J Biol Chem* 279(17), 17027-17037
63. Mal, T. K., Skrynnikov, N. R., Yap, K. L., Kay, L. E., and Ikura, M. (2002) *Biochemistry* 41(43), 12899-12906
64. Bhattacharya, S., Bunick, C. G., and Chazin, W. J. (2004) *Biochim Biophys Acta* 1742(1-3), 69-79

65. Ahmad, S., Martin, P. E., and Evans, W. H. (2001) *European journal of biochemistry / FEBS* 268(16), 4544-4552

FIGURE LEGENDS

Fig. 1. Membrane topology and predicted CaM binding sequences in Cx43. *A*, Transmembrane (TM) topology and the primary sequence of Cx43. The integral membrane protein Cx43 is composed of four TM regions (TM1-4), two extracellular loops, one cytoplasmic loop, a short N-terminus, and a longer C-terminal tail. The TM segments (black cylinders) were assigned using four prediction programs (13-16). The predicted high-affinity CaM binding site (aa 136-158, box II) of highest predicted score (12) is located in the second half of the intracellular loop between TM2 and TM3. Two other regions (boxes I and III) with lower predictive scores (12) are also identified. The numeric score ranges from 1-9, representing the probability of an accurate prediction of a high affinity CaM binding site. *B*, Helical wheel representation of the CaM binding site of highest score in Cx43. The identified CaM-binding sequence Cx43₁₃₆₋₁₅₈ fits the hydrophobic residue 1-5-10 subclass where each number represents the presence of a hydrophobic residue. #: hydrophobic residues. Basic charged residues are shown in *black*, whereas the hydrophobic residues are shown in *gray*.

Fig. 2. Far UV CD spectra of the synthetic peptide Cx43₁₃₆₋₁₅₈ (10 μM) with 0 (●), 10% (▲), 20% (◇), 40% (+), 60% (○), an 80% (□) TFE. The *inset* shows the changes of molar ellipticity at 222 nm and 208 nm as a function of TFE concentration.

Fig. 3. Circular Dichroism studies of the interaction between Cx43₁₃₆₋₁₅₈ and CaM. *A*, Far UV Circular Dichroism spectrum of CaM in the presence of 1 mM EGTA (○) or 1 mM CaCl₂ (□), and a 1:1 CaM-synthetic peptide mixture with 1 mM EGTA (●) or 1mM CaCl₂ (■) after subtracting the contribution from buffer and added peptides. Spectra were recorded at room temperature in 10 mM Tris, 100 mM KCl, pH 7.4. *B*, The far UV circular dichroism spectra of Cx43₁₃₆₋₁₅₈ (*dash line*) and the calculated difference spectrum (*solid line*) by subtracting the spectrum of Ca²⁺-CaM from that of the Ca²⁺-CaM-Cx43₁₃₆₋₁₅₈ mixture with 1 mM Ca²⁺ in a buffer consisting of 100 mM KCl, 10 mM Tris-HCl, pH 7.4. The inset reports the relative change of the circular dichroism molar ellipticity at 222 nm as a function of synthetic peptide concentration in buffer comprising 1 mM Ca²⁺, 100 mM KCl, 10 mM Tris-HCl, pH 7.4. All experiments were conducted in at least duplicate. *C*, Near UV circular dichroism spectra of CaM in the presence of 1 mM EGTA (○) or 1 mM CaCl₂ (□), and 1:1 CaM- Cx43₁₃₆₋₁₅₈ mixture with 1 mM EGTA (●) or 1mM CaCl₂ (■) after subtracting the contribution from buffer and added peptides. *D*, The near UV circular dichroism spectra of Cx43₁₃₆₋₁₅₈ (*dash line*) and the calculated difference spectrum by subtracting the Ca²⁺-CaM spectrum from the Ca²⁺-CaM- Cx43₁₃₆₋₁₅₈ spectrum (*solid line*) in a buffer consisting of 1 mM Ca²⁺, 100 mM KCl, 10 mM Tris-HCl, pH 7.4.

Fig. 4. Monitoring the interaction of CaM with Cx43₁₃₆₋₁₅₈ by surface plasmon resonance spectroscopy. The sensorgrams represent the binding of 0.5, 1, 5 and 10 μM Cx43₁₃₆₋₁₅₈ (A) or

10 μM of the randomized Cx43 peptide (*B*) to the CaM-immobilized chip in the presence of 5 mM Ca^{2+} (*solid line*) or EGTA (*dashed line*). CaM was immobilized to the sensor chip CM with a response unit of approximately 3500. The flow rate was set at 5 $\mu\text{l}/\text{min}$. During recording, running buffer contained 5 mM CaCl_2 or 5 mM EGTA in 100 mM KCl, 50 mM Tris-HCl at pH 7.4 or the same buffer plus the peptides (*solid bar*). Subsequently, peptide-free buffer was injected to monitor the dissociation process.

Fig. 5. Interaction of Cx43₁₃₆₋₁₅₈ with CaM or dansyl-CaM monitored by fluorescence spectroscopy. *A*, Tyrosine fluorescence spectra of Cx43₁₃₆₋₁₅₈ in the presence of 1 mM EGTA (*dashed line*) or 1 mM CaCl_2 (*solid line*), CaM in the presence of 1 mM EGTA (\circ) or 1 mM CaCl_2 (\square), and 1:1 mixture of CaM: Cx43₁₃₆₋₁₅₈ in 1 mM EGTA (\bullet) or 1 mM CaCl_2 (\blacksquare). *B*, Dansyl fluorescence spectra of dansyl-CaM (1.25 μM) in the presence of 1 mM EGTA (\circ) or 1 mM CaCl_2 (\square), and 1:1 mixture of CaM: Cx43₁₃₆₋₁₅₈ in 1 mM EGTA (\bullet) or 1 mM CaCl_2 (\blacksquare). *Inset*: the fluorescence intensity change at 490 nm plotted as a function of the peptide Cx43₁₃₆₋₁₅₈:CaM ratio. *C*, Dansyl fluorescence spectra of Ca^{2+} -dansyl-CaM (1.25 μM) in the absence (\square) and presence (\blacksquare) of the Cx43₈₈₋₁₀₇ peptide (2.5 μM) in 1 mM CaCl_2 . *D*, Dansyl fluorescence spectra of Ca^{2+} -dansyl-CaM (1.25 μM) in the absence (\square) and presence (\blacksquare) of the Cx43₂₂₂₋₂₄₇ peptide (2.5 μM) in 1 mM CaCl_2 .

Fig. 6. Interaction between CaM and Cx43₁₃₆₋₁₅₈ revealed by NMR. *A*, Overlaid HSQC spectra of Ca^{2+} -CaM (*green*) with Ca^{2+} -CaM-Cx43₁₃₆₋₁₅₈ (*red*) or Ca^{2+} -CaM:control randomized Cx43₁₃₆₋₁₅₈ peptide (*blue*). A subset of assigned peaks displaying significant movement upon peptide binding were framed in *boxes*. *B*, Overlay of HSQC spectrum of apo-CaM (*green*) with apo-CaM-Cx43₁₃₆₋₁₅₈ (*red*). *C*, Changes in chemical shift of selected well-dispersed resonances as a function of the Cx₁₃₆₋₁₅₈: Ca^{2+} -CaM ratio in the presence of saturating Ca^{2+} at physiological K^+ condition. *D*, 3-D representation of perturbed residues in Ca^{2+} -CaM (pdb: 3CLN) upon binding of the synthetic peptide Cx43₁₃₆₋₁₅₈. Residues with amide proton resonance changes over 0.05 ppm were shown in *red*.

Fig. 7. Effect of Cx43₁₃₆₋₁₅₈ on the Ca^{2+} affinity of CaM. Ca^{2+} titration of CaM (\circ), the 1:1 CaM:Cx43₁₃₆₋₁₅₈ mixture (\bullet), and the 1:1 CaM: randomized control peptide (\blacklozenge) in 100 mM KCl, 50 mM Tris-HCl, pH 7.3. The intrinsic tyrosine fluorescence emission intensity of CaM or CaM-peptide mixture (8 μM) was monitored at 307 nm with fluorescence excitation at 277 nm. The Ca^{2+} indicator dye Oregon Green 488 BAPTA-5N was used to calibrate the ionized Ca^{2+} concentration as described in “Experimental Procedures”. Each titration point is indicated as an open diamond at the bottom of the figure. Data from a single experiment representative of at least triplicate experiments.

Fig. 8. Functional effect of a sustained elevation in intracellular $[\text{Ca}^{2+}]$ on CaM binding-deficient Cx43-EYFP mutants. Cell-to-cell transfer of injected AlexaFluor 594 dye between HeLa cells transiently transfected with wtCx43-EYFP or the CaM-binding Cx43 mutants (Cx43_{K146E, R148E}-EYFP or Cx43_{M147Q, L151E, I156E}-EYFP) was measured in confluent monolayers of cells. Panels A-H show images of transiently transfected wt or mutant Cx43-EYFP or mock-transfected HeLa cells. The left image shows the EYFP fluorescence of the injected and adjacent cells, the middle image is the fluorescence of EYFP plus brightfield, and the images on the right are of AlexaFluor 594 dye transfer. Panels A&E: wtCx43-EYFP transiently transfected HeLa

cells; Panels B&F: Cx43_{K146E, R148E}-EYFP transiently transfected HeLa cells; Panels C&G: Cx43_{M147Q, L151E, I156E}-EYFP transiently transfected HeLa cells; Panels D&H: mock-transfected HeLa cells. Panel I: Summary data for cell-to-cell dye transfer (solid bars) and $[Ca^{2+}]_i$ (hatched bars) in the absence or presence of elevated $[Ca^{2+}]_i$. wtCx43-EYFP, resting $[Ca^{2+}]_i$: $0.075 \mu M \pm 0.01 \mu M$ and 100% of injections resulted in dye transfer (n = 5); elevated $[Ca^{2+}]_i$: $0.911 \mu M \pm 0.09 \mu M$ and 0% of injections resulted in dye transfer (n = 6). Cx43_{K146E, R148E}-EYFP, resting $[Ca^{2+}]_i$: $0.129 \mu M \pm 0.02 \mu M$ and 31% of injections resulted in dye transfer (n = 32); elevated $[Ca^{2+}]_i$: $1.77 \mu M \pm 0.31 \mu M$ and 57% of injections resulted in dye transfer (n = 7). Cx43_{M147Q, L151E, I156E}-EYFP, resting $[Ca^{2+}]_i$: $0.135 \mu M \pm 0.06 \mu M$ and 32% of injections resulted in dye transfer (n = 22); elevated $[Ca^{2+}]_i$: $1.54 \mu M \pm 0.24 \mu M$ and 67% of injections resulted in dye transfer (n = 6). Mock-transfected, resting $[Ca^{2+}]_i$: $0.073 \mu M \pm 0.01 \mu M$ and 0% of injections resulted in dye transfer (n = 3); elevated $[Ca^{2+}]_i$: $1.85 \mu M \pm 0.15 \mu M$ and 0% of injections resulted in dye transfer (n = 3). * indicates cell-to-cell dye transfer was significantly lower than cell-to-cell dye transfer determined in low $[Ca^{2+}]_i$; ** indicates $[Ca^{2+}]_i$ was significantly higher than the low $[Ca^{2+}]_i$ value.

TABLES

Table 1. The binding affinities of Cx43₁₃₆₋₁₅₈ to CaM or dansyl-CaM in the presence of 1 mM Ca²⁺.

KCl (mM)	Dissociation constants (K_d , nM)
10	100 ± 20^a 240 ± 10^b
100	750 ± 120^a 860 ± 20^b

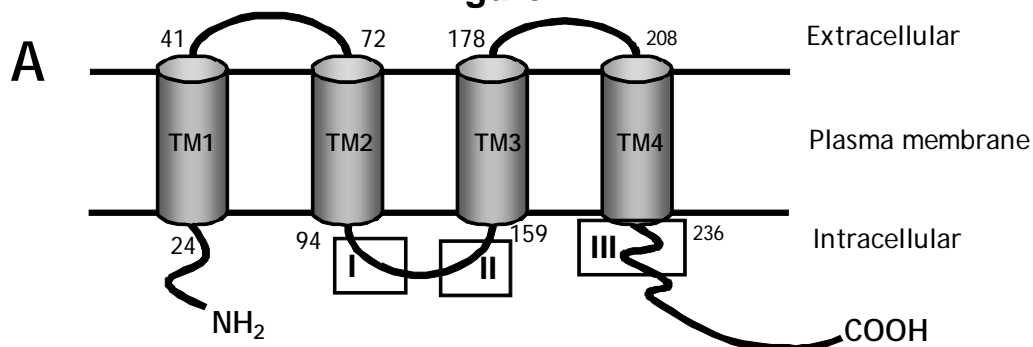
Data obtained from ^afar UV CD data (Fig.3) or ^bDansyl-CaM fluorescence (Fig. 5) (n=3-6).

Table 2. Effect of Cx43₁₃₆₋₁₅₈ binding on the Ca²⁺ binding affinity of CaM.

Sample	Fold enhancement		
	of tyrosine fluorescence	K_d (10^{-6} M)	n_{Hill}
CaM	2.3	2.9 ± 0.1	2.1 ± 0.1
1:1 CaM-randomized control peptide	1.9	2.7 ± 0.1	1.9 ± 0.2
1:1 CaM-Cx43 ₁₃₆₋₁₅₈	1.7	1.6 ± 0.1	3.3 ± 0.5

Data obtained from Ca²⁺ titration curve (Fig. 7) (n=3).

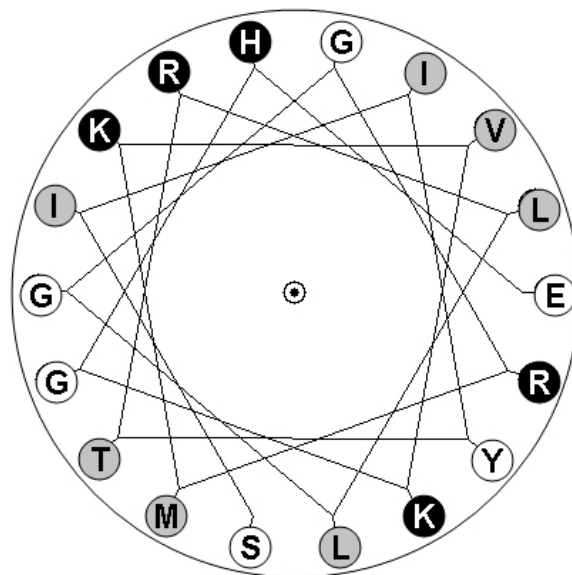
Figure 1



```

1
MGDWSALGKL LDKVQAYSTA GGVWLSVLF IFRILLLGTA VESAWGDEQS AFRCNTQQPG CENVCYDKSF
0000000000 0000000000 0000000000 0000000000 0000000000 0000000000 0000000000
71
PISHVRFWVL QIIFVSVPTL LYLAHVFYVM RKEEKLNKKE EELKVAQTDG VNVMHLKQI EIKKFKYGIE
0000000000 0000011233 3333333333 3333332110 0000000001 1111111111 1123345666
141
EHGKVKMRGG LLRTYIISIL FKSVEFAFL LIQWYIYGFS LSAVYTCKRD PCPHQVDCF LSRPTEKTIFI
7899999999 9987665433 2110000000 0000000000 0000000000 0000000000 0000000000
211
IFMLVVSLVS LALNIIELFY VFFKGVKDRV KGRSDPYHAT TGPLSPSKDC GSPKYAYFNG CSSPTAPLSP
0000000000 0000111111 1111111111 1111111000 0000000000 0000000000 0000000000
281
MSPPGYKLV T GDRNNSCRN YNKQASEQNW ANYSAEQNRM GQAGSTISNS HAQPFDFPDD SQNAKKVAAG
0000000000 0000000000 0000000000 0000000000 0000000000 0000000000 0000000000
351
HELQPLAIVD QRPSSRASSR ASSRPRPDDL EI
0000000000 0000000000 0000000000 00
  
```

B



```

Cx43 136 KYGIEEHGKVKMRGGLLRITYIIS 158
xxxxxxxxBxB#xxx#xBxx#xx
1 5 10
  
```

Figure 2

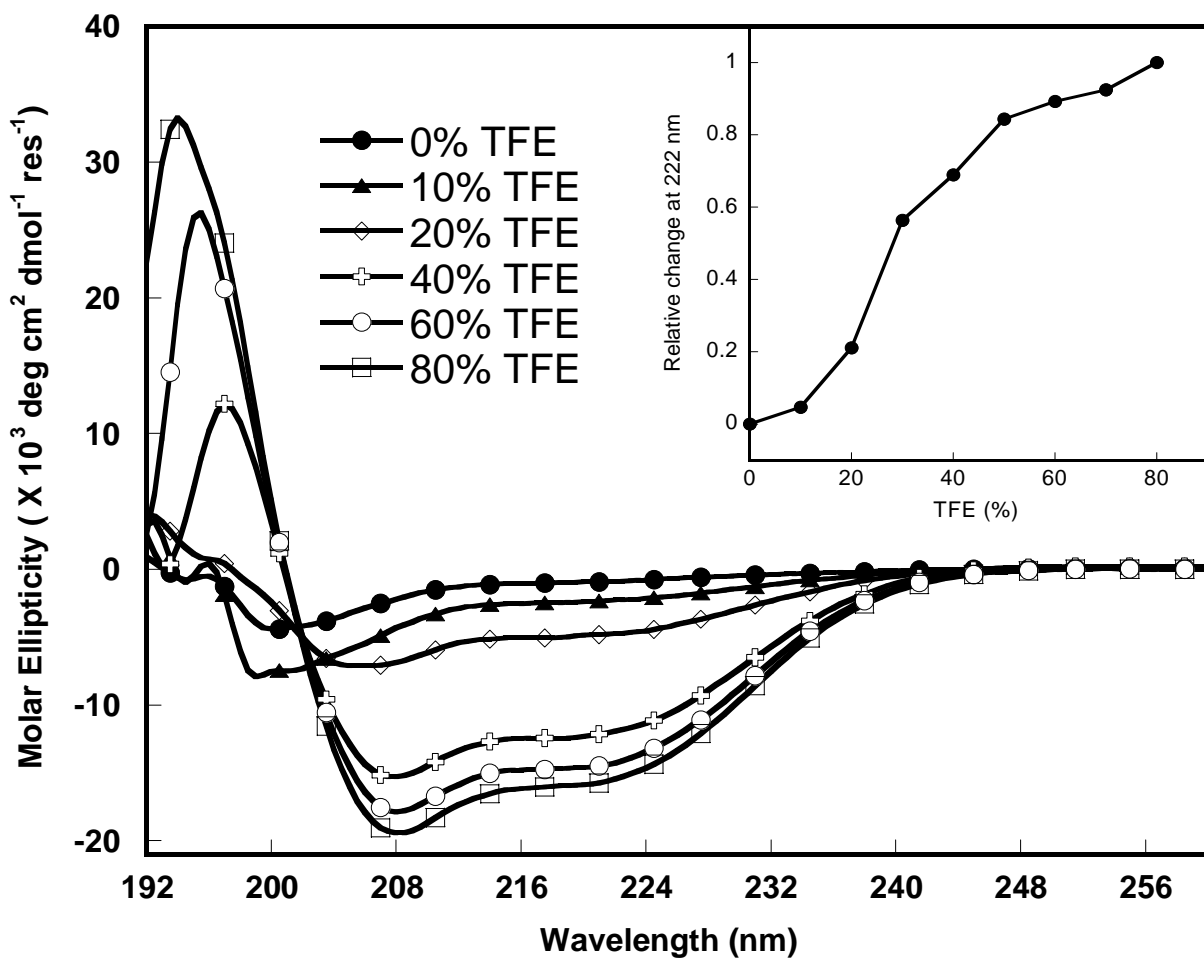


Figure 3

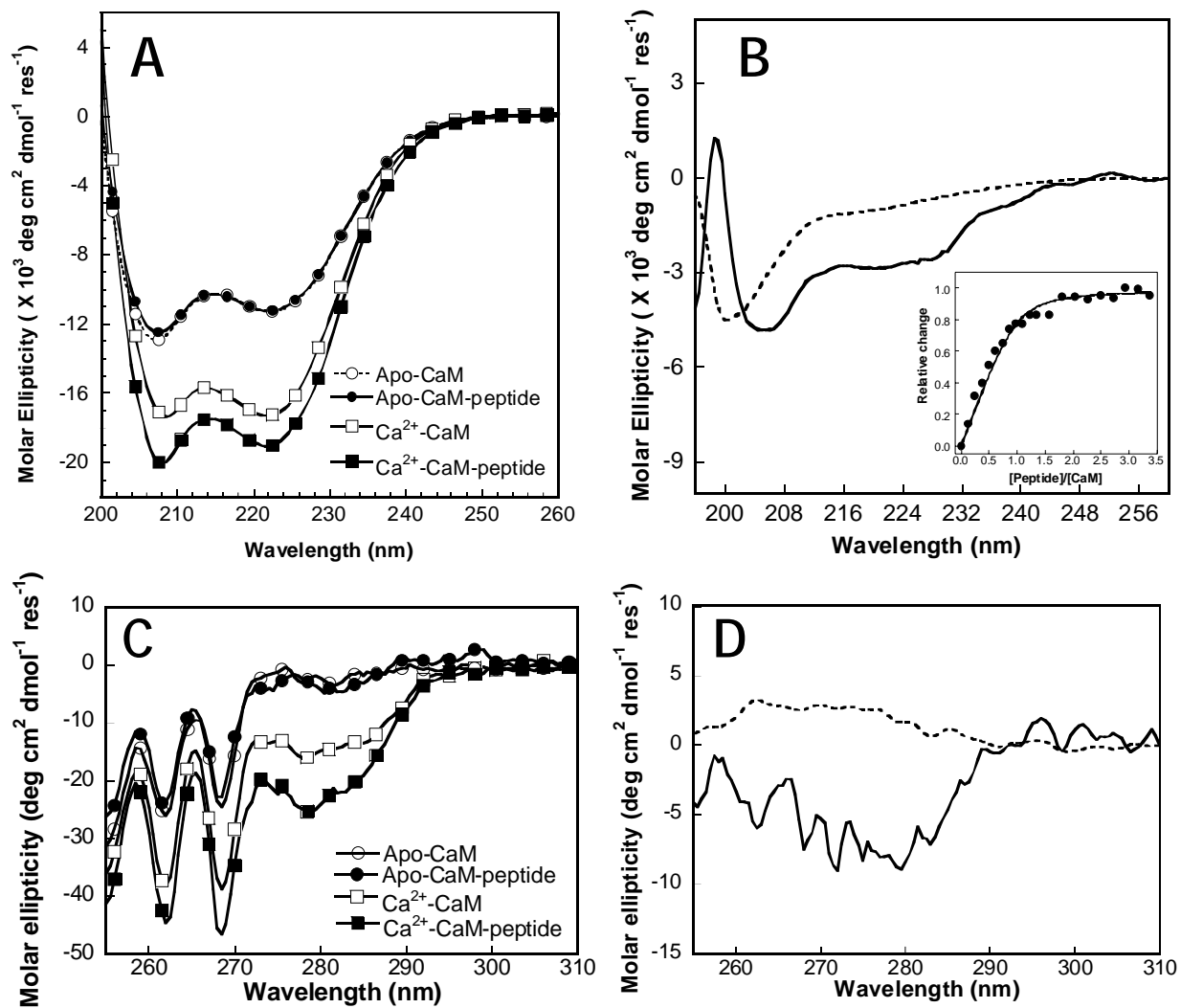


Figure 4

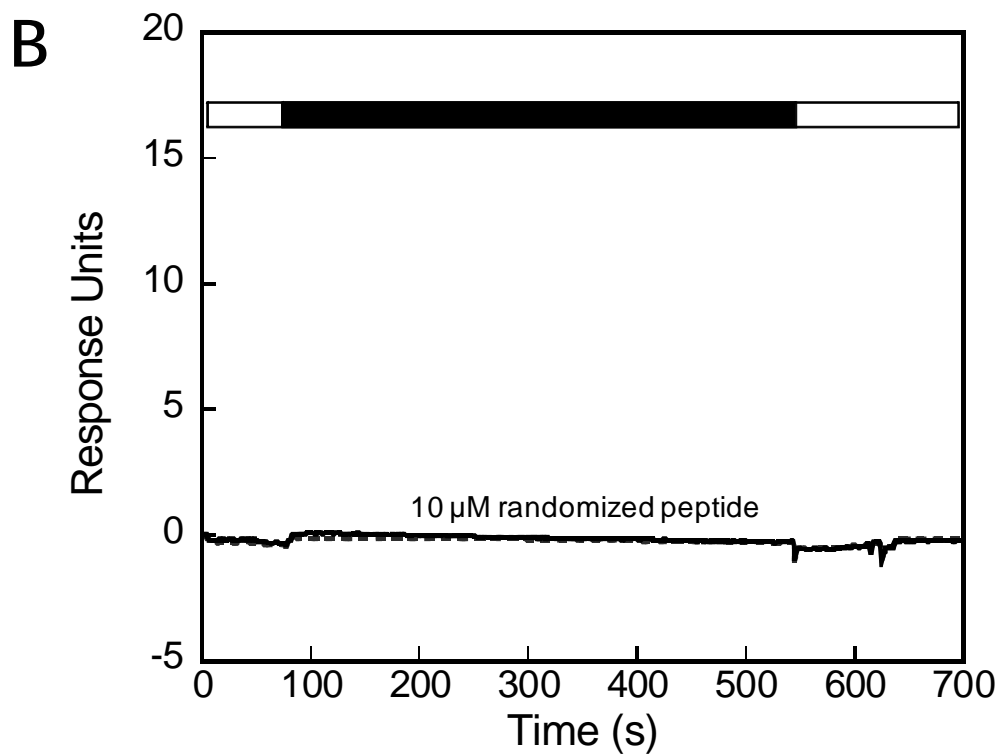
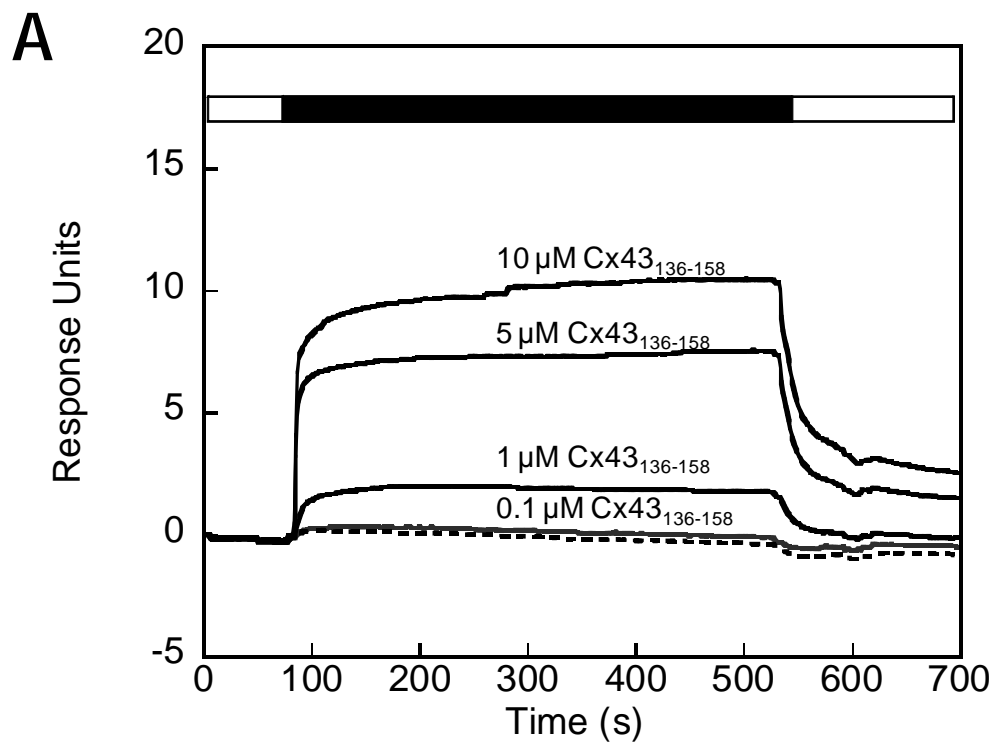


Figure 5 (A-B)

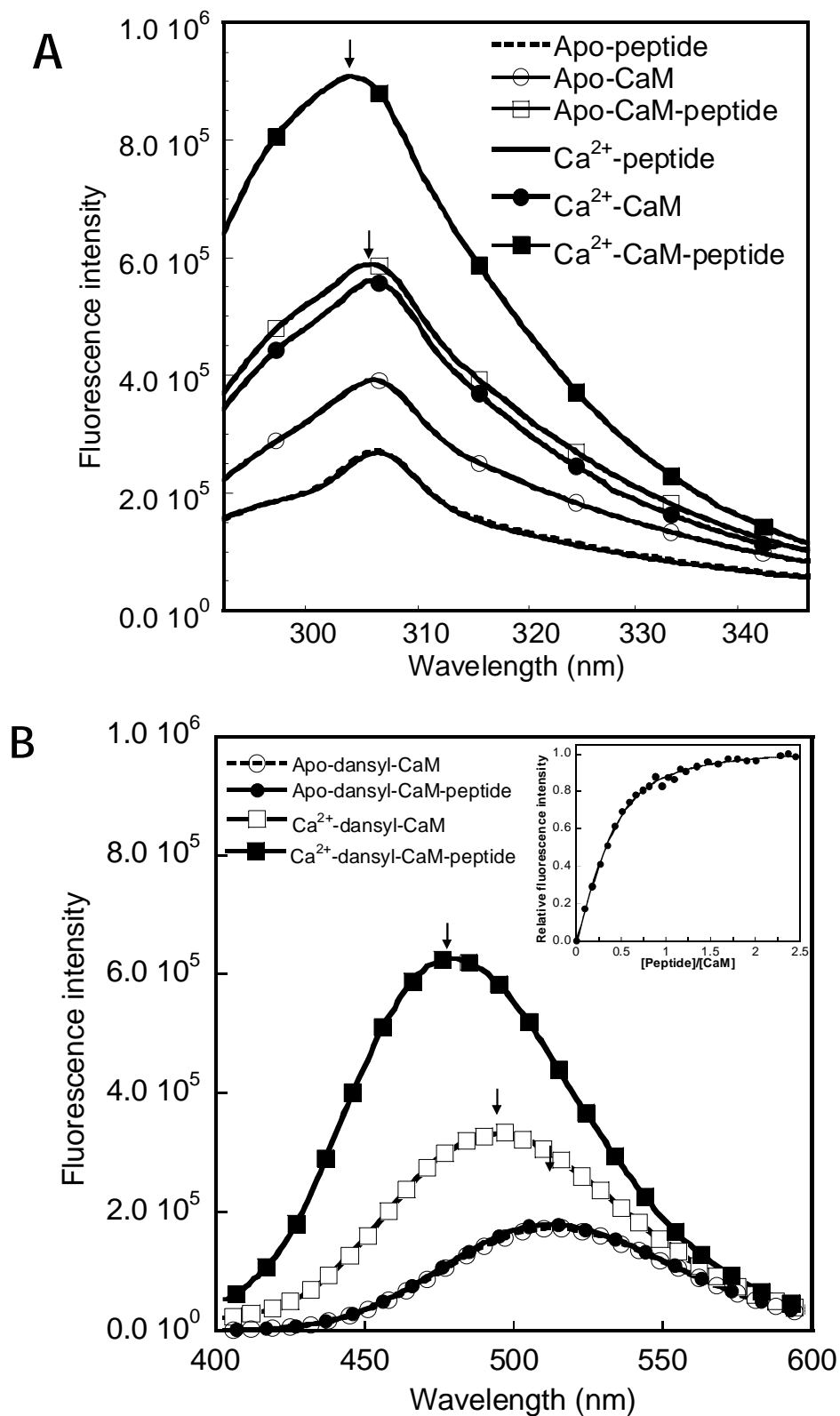
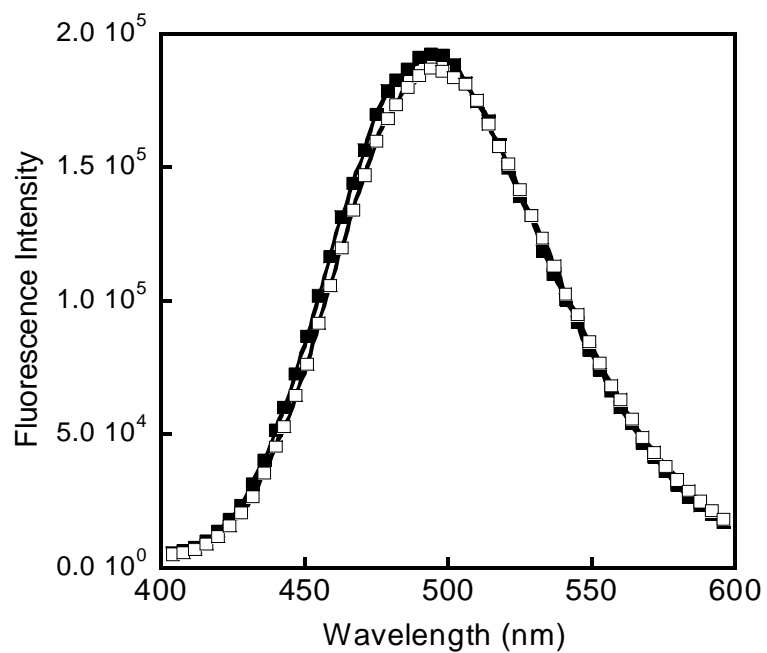


Figure 5 (C-D)

C



D

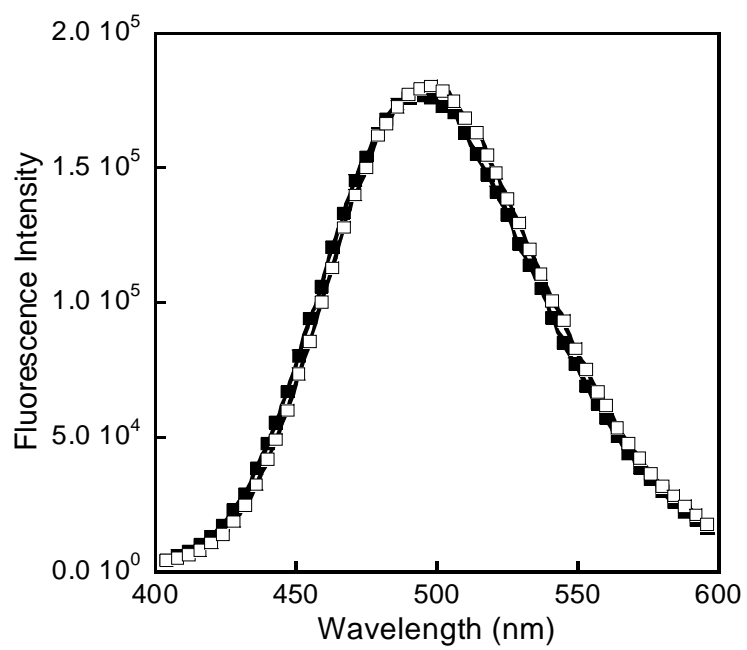


Figure 6 (A-B)

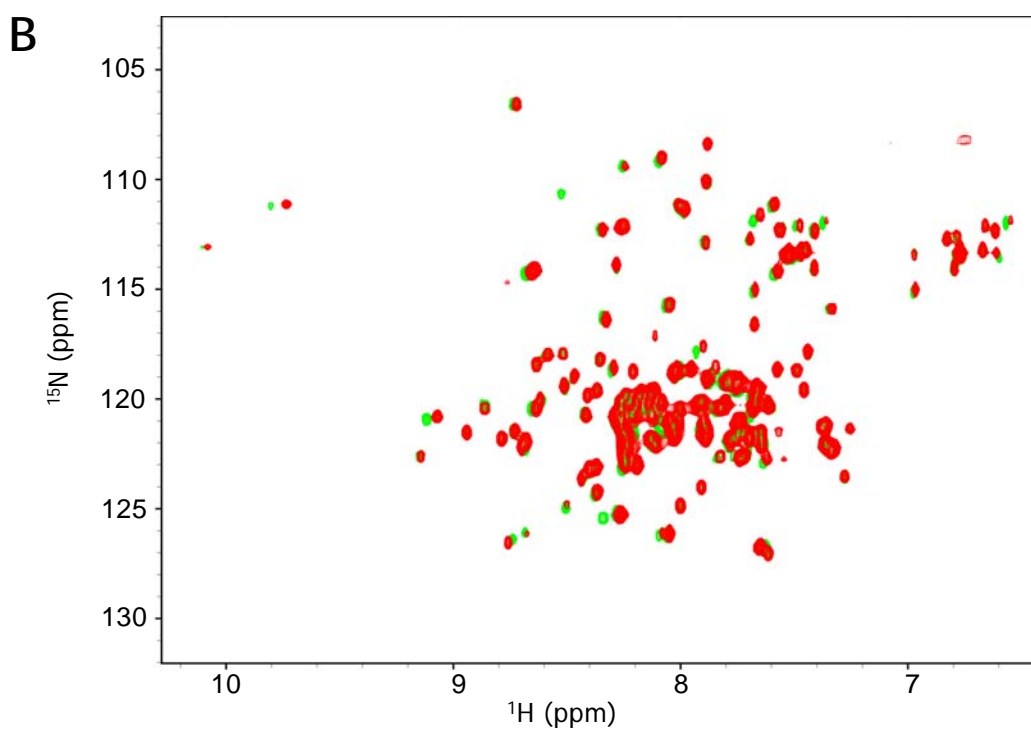
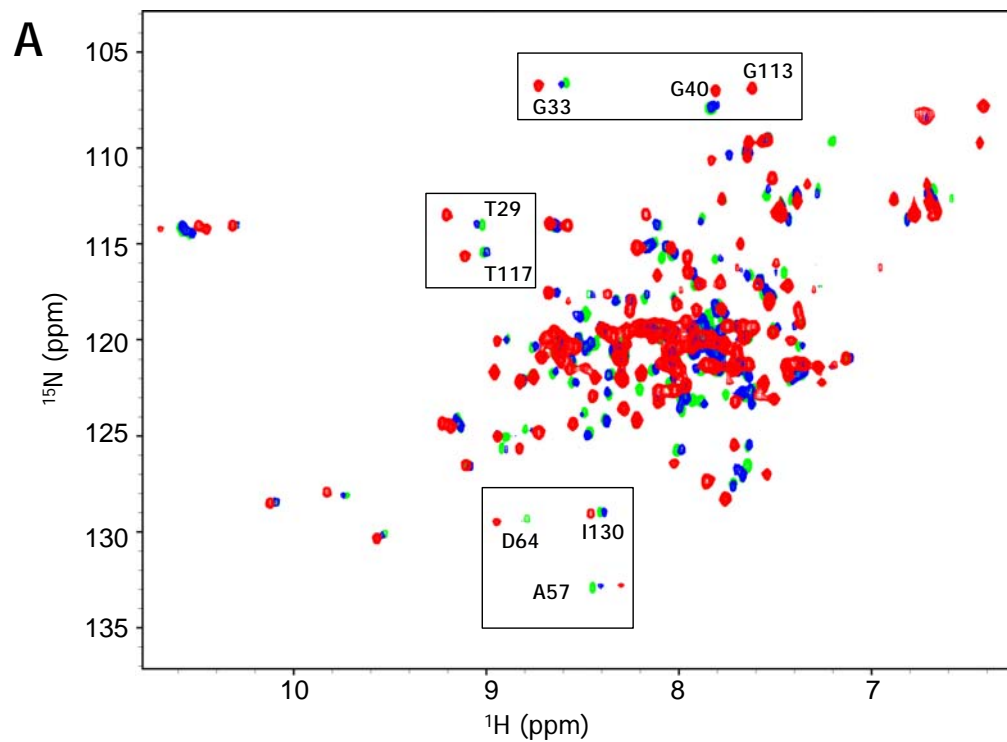
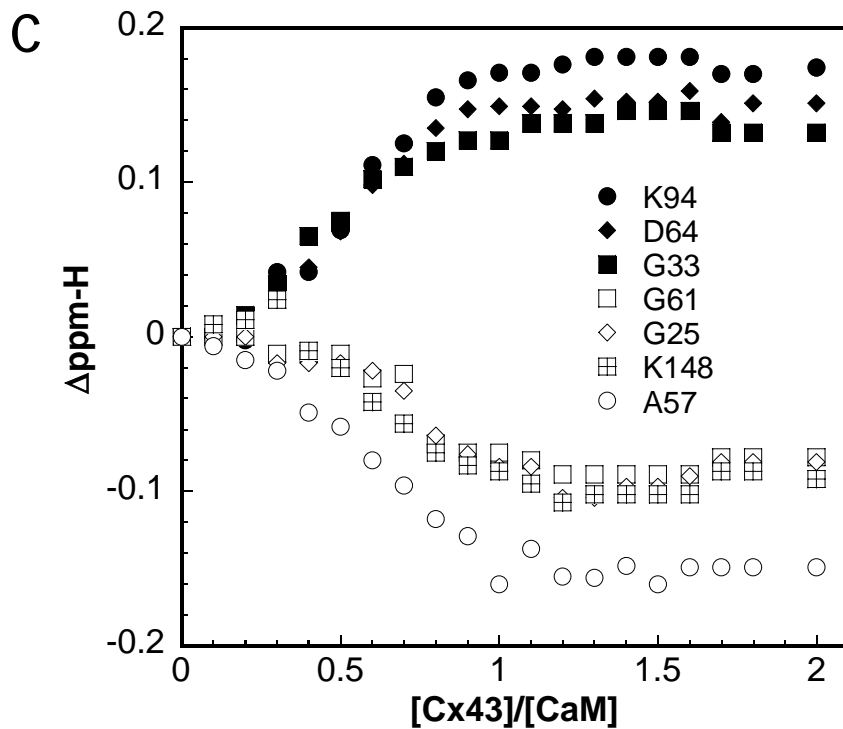


Figure 6 (C-D)



D

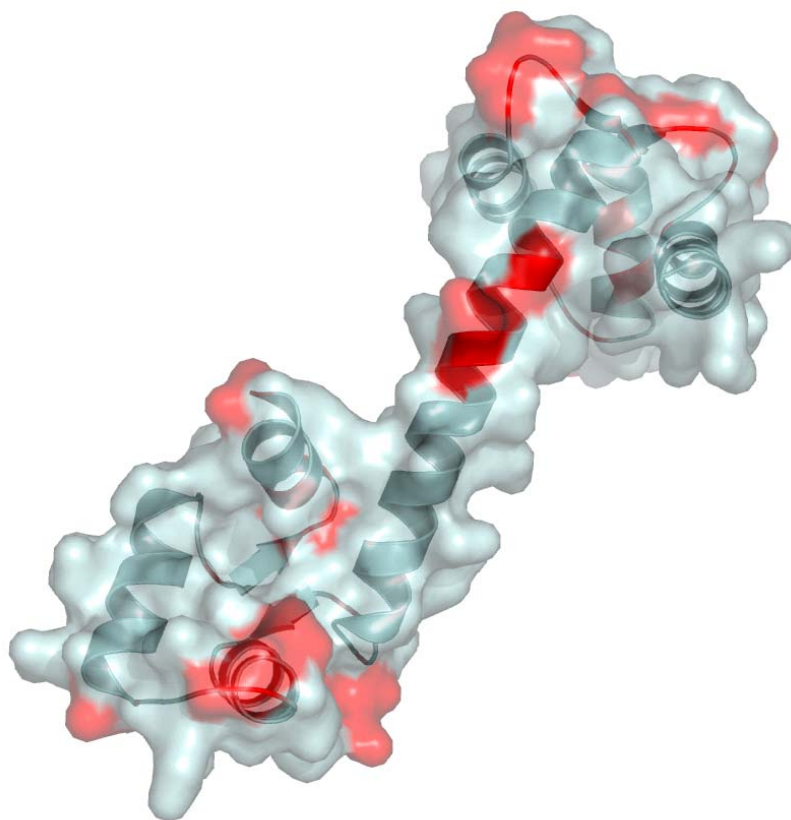


Figure 7

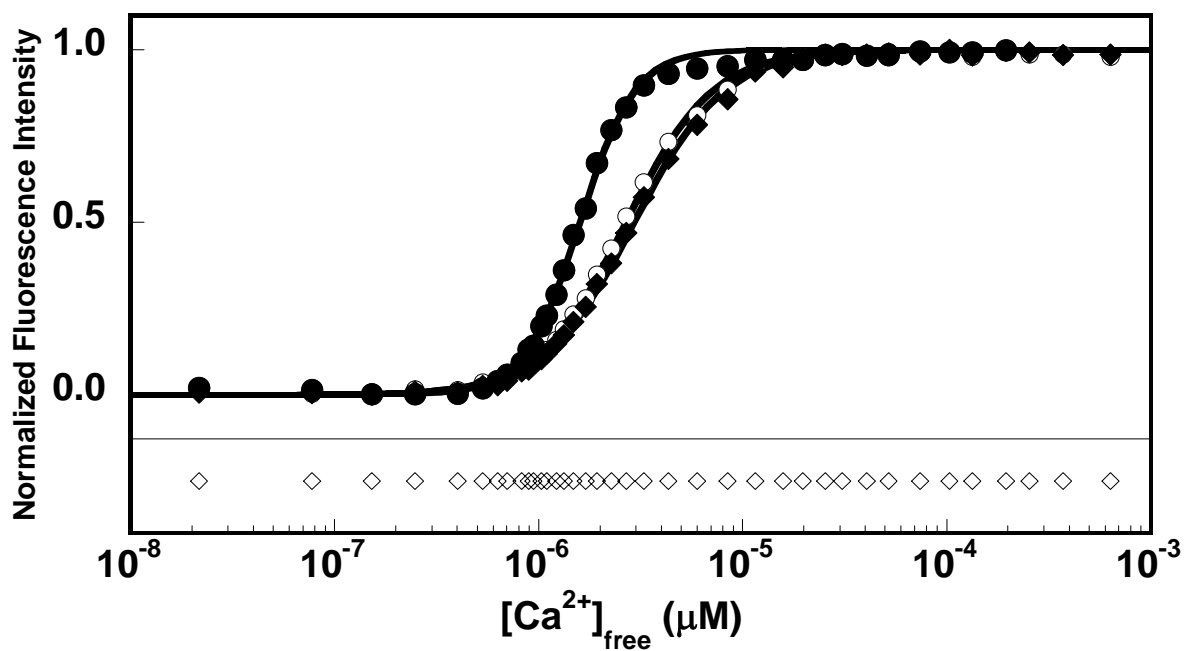
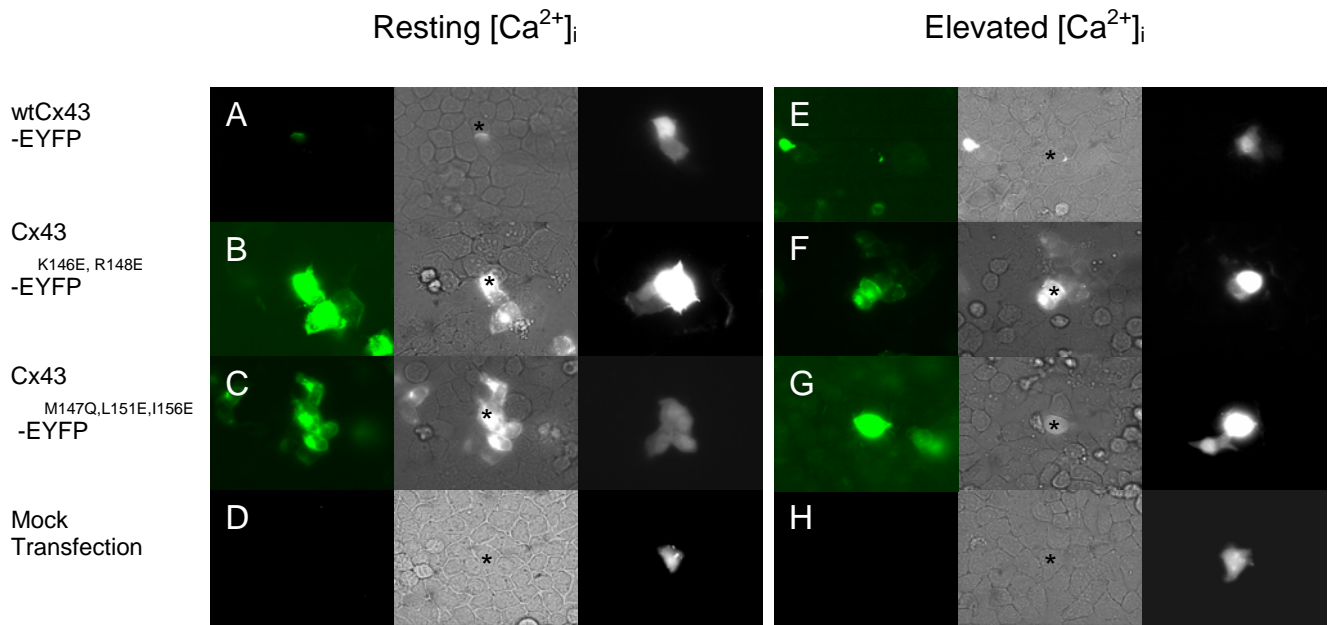


Figure 8



I

